Identification of select G-protein coupled receptors as regulators of the ER-mitochondria contacts by drug screening

Youngshin Lim[1#], Il-Taeg Cho[1#, 2], Helmut G. Rennke[1], and Ginam Cho[1*]

From the [1]Department of Pathology, Brigham and Women's Hospital and Harvard Medical School, Boston, MA 02115, USA.

Running title: Drug screen for ER-Mito contact enhancers

[2] Present address: Department of Surgery, Keck School of Medicine, University of Southern California, Los Angeles, CA 90033, USA.

[#] Equal contribution

[*] To whom correspondence should be addressed: gpcho@bwh.harvard.edu

Keywords: actin polymerization, β-adrenergic receptor (β-AR), calcium, CDC42, endoplasmic reticulum, mitochondria, EPAC, drug screening, G-protein coupled receptor (GPCR), split-*Renilla* luciferase.

ABSTRACT

Endoplasmic reticulum-mitochondrial (ER-Mito) contacts are crucial for many cellular functions. Their dysregulation has been implicated in various disorders including neurodegenerative, cardiovascular and metabolic diseases, and cancer. However, little is known about the regulatory pathways of ER-Mito contacts. To uncover such pathways, we screened a drug library using a split-*Renilla* luciferase (split-Rluc) reassembly assay in HEK293T cells. We identified multiple agonists of G-protein coupled receptors (GPCRs), beta-adrenergic receptors (β-ARs) in particular. Using multiple independent assays, we validated that these drugs enhance the physical and functional interactions between ER and mitochondria. Our data provide evidence that GPCR signal modulates ER-Mito coupling through activating EPAC (exchange protein directly activated by cAMP) and increasing cytoplasmic Ca^{2+} levels, and that actin polymerization, likely regulated by CDC42 upon receptor activation, is required for this coupling. Together our study identifies GPCR signaling as a regulatory mechanism for ER-Mito contacts, and highlights the role of these contacts in responding to physiological demands or stresses.

Introduction

In eukaryotic cells, membrane-bound organelles accomplish specialized functions in isolated compartments. For these organelles to communicate with each other, they use either vesicular trafficking systems requiring membrane fusion, or membrane contact sites where the membranes of interacting organelles become closely juxtaposed without fusion. While vesicular trafficking systems have been studied for a long time, membrane contact sites have only recently emerged as an active area of research (1-3).

ER-Mito contact is one of the most studied inter-organelle interactions (2, 4-7). In yeast, this contact is primarily tethered by the ER-mitochondria encounter structure (ERMES) complex that consists of four proteins: Mdm12, Mmm1, Mdm34, Mdm10) (4, 5). Similar contacts have been identified in mammalian cells, although the molecular identities of the mammalian tethering complex(es) are much more complicated and still debated (6-8). The function of the ER-Mito contact sites includes the transfer and metabolism of lipids (9, 10); modulation of Ca^{2+} fluxes and homeostasis (11, 12); formation of dynamic H_2O_2 nanodomains that regulate Ca^{2+} signaling (13); control of mitochondria fusion-fission dynamics (14, 15); biogenesis of autophagosomes and mitophagosomes (16, 17); and control of apoptosis (18). The failure to maintain normal ER-Mito contacts has emerged as a common feature of multiple human diseases (e.g., neurodegenerative, cardiovascular, and metabolic diseases, and cancer) (19-26). For example, we have shown that the disease-associated mutations in REEP1, linked to hereditary spastic paraplegia, result in decreased ER-Mito contacts when compared to wild type REEP1(23).

Although significant work remains, multiple studies suggest that both abnormal increases and decreases in ER-Mito contacts are detrimental to normal cellular functions (19). If ER-Mito contacts are abnormally enhanced, as observed in some Alzheimer's disease models (24-27), it has been postulated that the resulting mitochondrial Ca^{2+} overload would cause mitochondrial permeability transition pores (mPTP) to open, leading to mitochondrial swelling and cell death (28). On the other hand, if the contacts are abnormally reduced or disrupted, as in the cases of amyotrophic lateral sclerosis with associated frontotemporal dementia (ALS/FTD) models (29-32), the decreased contact is predicted to lower mitochondrial ATP generation (28), which in turn would drive motor neuron degeneration (33). Despite their implication in many diseases and the physiologic importance of maintaining their levels in the cell, little is known about how ER-Mito contacts are regulated.

We previously developed a split-*Renilla* luciferase (split-Rluc) reassembly assay to quantitatively measure the level of physical coupling between ER and mitochondria (23, 34). Our split-Rluc system consists of two separate DNA constructs, one encoding the N-terminal half of the *Renilla* luciferase with a mitochondrial targeting sequence (Mito-$Rluc^N$) and the other encoding the C-terminal half with an ER targeting sequence ($Rluc^C$-ER) (23). While each split construct by itself cannot generate luciferase activity, co-expression of both constructs results in full enzymatic activity at ER-Mito contact sites where the two

halves are closely apposed permitting reassembly and restoration of the luciferase activity. Although there are several established methods to detect ER-Mito contacts in cells (2, 3), our split-Rluc reassembly assay is optimal for drug screening, as it allows a simple high throughput detection of the ER-Mito contacts in live cells without artifacts associated with sample fixation or complications related to image analysis.

Using this split-Rluc assay in HEK293T cells, we screened an NIH clinical collection (NCC) of FDA approved drugs to identify compounds that could potentially enhance ER-Mito contacts. All 11 confirmed hits were agonists of G-protein coupled receptors (GPCRs) and 9 of them target beta-adrenergic receptors (β-ARs). Our data reveal for the first time that GPCRs act as a regulatory signaling for ER-Mito contacts. Given the role of GPCRs in sensing various extracellular signals (e.g., photons, ions, lipids, amines, peptides, growth factors, and hormones) (35) and subsequently eliciting appropriate cellular responses, our data provide significant insights into the roles of ER-Mito contacts in maintaining cellular homeostasis and in responding to physiological demands (or stresses) such as increases in mitochondrial ATP generation, alterations in lipid production, and/or autophagy induction. Moreover, our findings identify a novel mechanism of action for β-AR agonists, drugs shown to be associated with decreased risk in Parkinson's disease (PD) and beneficial to several PD models (36-38). This also opens up possibilities for therapy of other conditions known to have a component of the disease process associated with defects in ER-Mito contacts.

Results

Screening FDA-approved drugs for ER-Mito contact enhancers using split-Rluc reassembly assay.

To identify compounds that enhance ER-Mito contacts, we screened a library of 720 FDA-approved investigational drugs (NIH Clinical Collection, NCC) with the split-Rluc reassembly assay (Fig. 1) (23, 34). HEK293T cells expressing split-Rluc constructs were treated with DMSO (control) or each drug at 1 μM final concentration for 5 hours (Fig. 1A, B). The luciferase activities in live cells were measured using EnduRen™ as a substrate and normalized by the quantile method (39). From the initial screen, we identified 32 hits (4.4% hit rate) using the cut-off value of 3 standard deviation (SD) above the average of the control (Fig. 1C; Table S1). These hits were found to target GPCRs (19 drugs, 59% of the 32 hits); glucocorticoid receptors (5 drugs, 16% of the 32 hits; labeled as steroid); DNA topoisomerases/polymerases (5 drugs, 16% of the 32 hits; labeled as DNA related); and others (3 drugs, 9% of the 32 hits) (Fig. 1C; Table S1).

Given the high percentage (59%; 19 of 32) of the GPCR-linked drugs among our initial hits, we focused on these 19 drugs. We repeated the split-Rluc assay and confirmed positive results for 11 compounds that showed consistent, significant increase in split-Rluc activity (reconstituted luciferase activity) compared to DMSO control (Fig 2B). Why some drugs (e.g., triamcinolone; Table S1) showed higher activity in the

initial screen but not in the repeated assays remains uncertain. Of note, we established that the positive hits did not alter the expression of the split-Rluc proteins (data not shown). Among 11 of these 'confirmed hits', 9 of them target ARs and the other two, alprostadil (a.k.a. prostaglandin E1, PGE1) and 2-chloro-N^6cyclopentyladenosine (CCPA), target prostaglandin and adenosine receptor pathways, respectively (Fig. 2C). Considering that only 18% (59 of 331) of the GPCR-linked drugs and 8% (59 of 720) of the total drugs in this library target ARs (Fig. 2A; Table S2), these data indicate an enrichment of AR-associated drugs in our screen.

Out of the 9 AR agonist hits, 7 of them are specific for β-ARs—isoproterenol (a.k.a. isoprenaline), metaproterenol, and duvadilan are non-selective β-AR agonists; terbutaline, salmeterol, formoterol, and salbutamol are specific to β2-AR (https://pubchem.ncbi.nlm.nih.gov/) (Fig. 2C)—while the other two, epinephrine and norepinephrine, activate both α- and β-ARs. Interestingly, while these 9 hits are all agonists of β-ARs (epinephrine and norepinephrine activate both α- and β-ARs), all other AR-associated compounds not identified as hits either target α-ARs (agonists/antagonists) or are annotated as antagonists of β-ARs (Fig. 2D; Table S3). These findings demonstrate that our screen successfully identified drugs that specifically activate β-ARs. Taken together, these data indicate that the activation of GPCRs, especially β-ARs, likely play a key role in modulating ER-Mito contacts.

To explore receptor pharmacology, we first tested for a concentration dependency of the drug effect, by measuring the split-Rluc activities in HEK293T and HeLa cells treated with different concentrations of isoproterenol, a selected drug with the highest response (see Fig. 2B). Similar concentration-response curves in these two cell lines were obtained (Fig. 2E and S1A). In addition, isoproterenol response was also tested in C2C12 (mouse myoblasts) and Neuro2a (mouse neuroblastoma) cells. While C2C12 cells were responsive to isoproterenol like HEK293T and HeLa cells (Fig. S1B), Neuro2a cells were not, suggesting a cell-line dependent response (Fig. S1C). This is likely due to the differences in receptor availability in these cell lines: Neuro2a cells have little or no β-AR expression, unlike the other two cell lines (see Table S4 for mRNA-seq results for GPCRs; β-ARs are in red color). Next, we tested for a receptor specificity by investigating if the isoproterenol activity could be blocked by β-AR antagonist. Sotalol (β-AR antagonist) treatment abolished the effect of isoproterenol (Fig. 2F), confirming the specificity of β-AR in isoproterenol-mediated ER-Mito coupling.

Finally, to validate the increase in split-RLuc activity is not exclusively the result of enhanced split-Rluc expression, we measured the effect of the selected drug (isoproterenol) with or without the transcription inhibitor actinomycin D (Fig. 2G). In cells treated with actinomycin D alone, split-Rluc activity was lowered (suggesting some ER-Mito contact is in part influenced by transcription inhibition). However, isoproterenol treatment significantly lifted the inhibitory effect of actinomycin (Fig. 2G),

demonstrating that the isoproterenol-induced split-Rluc activity indeed resulted from the elevated level of the physical tethering between the two organelles and not as a result of increased gene expression alone.

GPCR agonists, isoproterenol, CCPA, and PGE1, increase physical contact between ER and mitochondria.

As noted above, three classes of confirmed hits were identified among the 720 compounds. We selected one member from each class to further investigate a potential role in ER-Mito contacts. Isoproterenol is a β-AR agonist (https://pubchem.ncbi.nlm.nih.gov/compound/3779) and was selected out of the 9 AR agonist hits because it showed the highest activity (Fig. 2B); CCPA is a specific agonist for the adenosine A1 receptor (https://pubchem.ncbi.nlm.nih.gov/compound/123807); and PGE1 is specific for the prostaglandin E2 receptor subtypes EP1 and EP2 (https://pubchem.ncbi.nlm.nih.gov/compound/5280723).

In order to corroborate our split-Rluc assay results and validate that the selected drugs can indeed enhance physical contact between ER and mitochondria, we employed two independent assays. First, we used an *in situ* proximity ligase assay (PLA), which is based on the labeling of two proteins present in close proximity in fixed cells with specific primary antibodies and oligonucleotide-linked secondary antibodies (40). Primary antibodies against ER protein SEC61-GFP and mitochondrial protein TOM20 were selected. When SEC61 and TOM20 are in sufficient proximity (i.e., ER-Mito contact is formed), subsequent ligation and rolling circle amplification reactions lead to a fluorescent product (red) that can be detected *in situ* (Fig. 3A). We found that the PLA fluorescence signals from the HeLa cells treated with isoproterenol, CPA, or PGE1 (1 μM each) were significantly higher than those treated with DMSO, supporting that these drugs indeed raise ER-Mito contacts (Fig. 3A, B).

Next, we assessed ER-Mito contacts at the ultrastructural level by transmission electron microscopy (TEM). HEK293T cells treated with DMSO or isoproterenol (1 μM) for 30 min were fixed and processed for TEM, and electron micrographs were used to determine the extent of ER-Mito contacts. The percentage of mitochondria juxtaposed (< 30 nm) to ER in isoproterenol treated cells was higher than in DMSO treated cells (DMSO, 22.5%; isoproterenol, 41.7%; $p < 0.0001$; Chi-square test) (Fig. 3C, D). Together, these data corroborate our results with the split-Rluc assay and demonstrate these compounds indeed increase the physical contacts between the two organelles.

GPCR agonists, isoproterenol, CCPA, and PGE1, enhance functional coupling between ER and mitochondria.

We next asked if the drug-induced physical contact between ER and mitochondria created functional coupling between these organelles. Given the previous studies that established the ER-Mito contact sites as

hotspots for Ca^{2+} influx to mitochondria (11, 28, 41), we investigated if the drug treatment could increase mitochondrial Ca^{2+} influx. To quantify Ca^{2+} levels in the mitochondria, we utilized a fluorescent Ca^{2+} sensor, mito-R-GECO1 (42, 43). HeLa cells were pre-treated with DMSO or one of the three drugs: isoproterenol, CCPA, and PGE1 (1 μM each). Mitochondrial Ca^{2+} uptake was then measured in response to histamine-stimulated ER Ca^{2+} release every 2.5 seconds (Fig. 4A). Upon ER Ca^{2+} release, all three drugs, compared to DMSO, resulted in a higher maximum peak (Fig. 4A, B) and faster uptake rate (Fig. 4A, C) of mitochondrial Ca^{2+}. These data demonstrate that they triggered elevated and accelerated mitochondrial Ca^{2+} responses when compared to control. Thus, these drugs increased not only physical, but also functional coupling between ER and mitochondria.

Several lines of evidence indicate that ER-Mito contact contributes to mitochondrial bioenergetics by supplying Ca^{2+} to mitochondria (28, 44-46)(6, 47-49), because proteins involved in Krebs cycle and oxidative phosphorylation can be activated by Ca^{2+} (46-49). Accordingly, we next investigated if facilitated Ca^{2+} uptake by drug treatment would increase mitochondrial bioenergetics. For this purpose, we measured the mitochondrial membrane potential (Fig. 4D, E), an indicator of increased mitochondrial metabolism (50). Tetramethyl rhodamine methyl ester (TMRM) fluorescence dye was used to determine mitochondrial membrane potential (51). We found increases in mitochondrial membrane potential (Fig. 4E) in isoproterenol treated cells. These findings imply that drug-induced ER-Mito contacts lead to enhanced mitochondrial metabolism via facilitated ER-to-mitochondria Ca^{2+} transfer.

cAMP/EPAC pathway mediates β-AR agonist-induced ER-Mito contact.

GPCRs transduce their signals through G proteins consisting of three subunits, α, β, and γ (Fig 5A). Upon GPCR activation, α subunit can dissociate from β/γ to affect other molecules in the cell depending on its subunit type: $G_{\alpha s}$, $G_{\alpha i}$, $G_{\alpha q}$, and $G_{\alpha 12}$ (35, 52). $G_{\alpha s}$ relays a signal to adenylate cyclase (AC) to generate cAMP whose downstream effectors include PKA family and EPAC (exchange protein directly activated by cAMP) which acts as guanine nucleotide exchange factor for small G proteins (RAP1 and RAP2); $G_{\alpha i}$ works by inhibiting adenylate cyclase; the effector of $G_{\alpha q}$ is phospholipase C_β (PLC_β) which cleaves PIP2 into IP3 and DAG, eliciting calcium release from ER and activating PKC; and the effectors of $G_{\alpha 12}$ are RhoGEFs which activate small GTPase Rho. In addition, GPCRs can also activate MAPK cascades via G protein independent signaling (e.g., β-arrestin) as well as $G_{\beta\gamma}$ complex dissociated from G_α (53-55).

To determine which downstream factors are involved in ER-Mito contact modulation by β-AR, we first evaluated $G_{\alpha s}$-mediated pathway. Using a cAMP response element (CRE) reporter gene assay (a proxy for cAMP measurement) in HEK293T cells, we detected an increase in cAMP level upon isoproterenol treatment (fold change: 4.79 ± 1.66) compared to DMSO (Fig. 5B), confirming $G_{\alpha s}$/AC pathway activation.

Corroborating this result, the expression of a constitutively active mutant construct for $G_{\alpha s}$ ($G_{\alpha s}$ CA), which can activate the signaling cascade even in the absence of ligand (56), augmented split-Rluc activity compared to a control vector, while a constitutively active mutant construct of $G_{\alpha i}$ ($G_{\alpha i}$ CA) reduced it (Fig. 5C). Interestingly, when β2-AR itself was overexpressed, it induced much higher CRE reporter activity (fold change: 249.60 ± 19.90) (Fig. S2A) than isoproterenol, suggesting that the isoproterenol-mediated β-AR stimulation in our current assay system is not as strong as full activation via receptor overexpression.

Since cAMP can transduce signal through two different downstream effectors, PKA and EPAC, we tested each pathway. When the activity of EPAC was inhibited by ESI 09, luciferase reassembly was significantly reduced in the cells treated with DMSO or isoproterenol (Fig. 5D, left), strongly supporting that EPAC is required for ER-Mito coupling. Furthermore, when the isoproterenol-induced luciferase activities (fold change of the isoproterenol over DMSO) were compared between the vehicle- vs. ESI 09-treated cells, ESI 09 treated cells showed a significant reduction (Fig. 5D, right). This result indicates that EPAC activity is required for isoproterenol-induced ER-Mito contacts. Interestingly, however, RAP1A (EPAC downstream effector) activity does not appear to be required, as RAP1A dominant negative mutant (DN) expression did not cause any reduction in luciferase activity (Fig. 5E). Together these results suggest that EPAC might function in a RAP1A-independent manner for this role.

In line with our data, a recent study has demonstrated that EPAC is necessary for increasing the interaction between VDAC1, IP3R1, and GRP75, a well-established complex in ER-Mito contact sites (57). This, together with our data, strongly suggests that isoproterenol-induced EPAC activity might enhance ER-Mito tethering by facilitating the interaction between VDAC1, IP3R1 and GRP75.

In contrast to EPAC, the inhibition of PKA activity, by Rp-cAMPS and H-89, did not change the isoproterenol response (Fig. 5F, G), supporting that PKA might not participate in this response.

Next, to evaluate a possible activation of $G_{\beta\gamma}$ mediated pathway, we treated HEK293T cells with the MEK inhibitor, PD 032509, with or without isoproterenol, and measured the split-Rluc activity; no blocking effect of PD032509 on isoproterenol response was observed but rather a positive effect was noted (Fig. S2B). This result suggests that the MAPK pathway might not be necessary but rather it might exert a negative effect normally, although further investigation is required.

Elevated cytosolic* Ca^{2+} *enhances ER-Mito contact level.

In addition to its known coupling to $G_{\alpha s}$, β2-AR has been recently shown to couple to $G_{\alpha q}$ as well (52), which prompted us to next evaluate the $G_{\alpha q}$-mediated pathway in β2-AR signaling. First, we asked if isoproterenol treatment could lead to an increase in cytoplasmic Ca^{2+}, which is a downstream effector of $G_{\alpha q}$. Upon isoproterenol application to HeLa cells transfected with GCaMP6s (fluorescent Ca^{2+} sensor), we

detected an elevation of the cytoplasmic Ca^{2+} level, suggesting a $G_{\alpha q}$/PLC pathway activation. Interestingly, however, this increase was weaker than that induced by histamine (which stimulates Ca^{2+} release from ER via IP3R activation through $G_{\alpha q}$/PLC/IP3 pathway; histamine receptor is a GPCR) (Fig. 6B), suggesting a lower level of $G_{\alpha q}$/PLC/IP3 pathway activation by isoproterenol than by histamine.

Next we asked if $G_{\alpha q}$ activation itself could induce ER-Mito interactions, by taking advantage of a constitutively active $G_{\alpha q}$ mutant construct ($G_{\alpha q}$ CA) which can transduce signal without ligand stimulation. Notably, $G_{\alpha q}$ CA expression led to a significant increase in split-Rluc reassembly (fold change: 2.08 ± 0.12) (Fig. 6A), indicating that $G_{\alpha q}$ activation is sufficient to enhance ER-Mito coupling even in the absence of agonist.

Another question we sought out was: Is $G_{\alpha q}$ activation, then, required for isoproterenol-induced coupling? To test this, we treated HEK293T cells with a recently identified Gq inhibitor, ebselen, which binds to $G_{\alpha q}$ and inhibits Ca^{2+} increase triggered by receptor activation (58). Ebselen eliminated the positive effect of isoproterenol (Fig 6C), indicating that $G_{\alpha q}$ activation is indeed required for isoproterenol-induced ER-Mito coupling. However, considering its multiple inhibitory function, we cannot rule out the possibility of ebselen inhibiting other factors (e.g., PKC) that might crosstalk with $G_{\alpha s}$-pathway components (59) or other pathways.

Unlike ebselen, the PLC inhibitors edelfosine and U73122 showed rather mild inhibition (Fig. 6D, E; left). When the fold changes of the isoproterenol-induced luciferase activity (over DMSO) were compared between the vehicle- vs. each drug- treated cells, edelfosine showed a trend toward blocking isoproterenol response ($p = 0.0674$) although the effects of both drugs did not reach statistical significance (Fig. 6D, E; right). These data suggest that PLC activity might play a relatively minor role in isoproterenol signaling (for ER-Mito coupling).

Finally, we investigated if intracellular Ca^{2+} increase itself could enhance ER-Mito interaction. For this, we assessed the effects of the three different drugs, histamine, ionomycin and cyclopiazonic acid (CPA), all of which are known to elevate cytosolic Ca^{2+} concentration albeit by distinct mechanisms (60, 61). Histamine stimulates cytosolic Ca^{2+} release from the ER through IP3 receptor activation (60); ionomycin, a membrane permeable Ca^{2+} ionophore, allows both Ca^{2+} release from intracellular stores and extracellular Ca^{2+} influx to the cytoplasm (60); and CPA, a sarco-endoplasmic reticulum Ca^{2+}-ATPase (SERCA) inhibitor, blocks the uptake of Ca^{2+} ions back to the sarcoplasmic reticulum (SR)/ER lumen after their release into the cytosol, thus accumulating Ca^{2+} in the cytoplasm (61). All three drugs elevated Split-Rluc activity (Fig. 6F), demonstrating that increasing cytoplasmic Ca^{2+} concentration is sufficient to enhance ER-Mito contacts (of note, thapsigargin (0.1-10 μM), another SERCA inhibitor, did not enhance luciferase activity (data not shown), although at present the reason for this discrepancy remains uncertain. Our

findings with the split-Rluc assay were corroborated using *in situ* PLA. Upon histamine or ionomycin treatment, PLA fluorescence signal was increased when compared to DMSO control (Fig. 6G). Of note, the NCC library includes histamine pathway-related drugs belonging to GPCR associated drugs (Fig 2A; Table S2) but not identified as potential hits in our screen most likely because all of them are annotated as antagonists (Table S2).

Actin polymerization is required for isoproterenol-mediated ER-Mito contact regulation.

We next explored how cytosolic Ca^{2+}- and cAMP-increases can influence ER-Mito interaction. Previous reports have shown that multiple stimuli leading to cytosolic Ca^{2+} spike, such as ionomycin and histamine, trigger a transient surge in cytosolic actin polymerization (62, 63). Also, a recent study has reported that actin polymerization is required for ER-Mito contacts that result in mitochondrial Ca^{2+} uptake (60). Therefore, we hypothesized that an actin polymerization 'burst' (achieved through cytosolic Ca^{2+} rise and/or other means upon β-AR activation) would be required for isoproterenol-induced ER-Mito interaction. To test this hypothesis, we assessed the effect of latrunculin A (actin polymerization inhibitor) on isoproterenol-induced ER-Mito contacts. Latrunculin A completely abolished the positive effect of isoproterenol (Fig. 7B), supporting our hypothesis.

In the cell, actin reorganization is mainly regulated by RHO GTPases, with CDC42, RAC, and RHO being the most prominent members among them (Fig. 7A). It is well-established that the activation of CDC42, RAC, and RHO promotes actin polymerization (Fig. 7A) (64). These RHO GTPases are regulated by GEFs (guanine nucleotide exchange factors), GAPs (GTPase activating proteins) and GDIs (guanine nucleotide dissociation inhibitors); and the GPCR signaling is linked to the activation of these regulators (65, 66). In addition to $G_{\alpha 12}$-mediated pathway which is well-known for regulating RHO GTPases through RHO GEFs, intracellular Ca^{2+} increase (via activating calmodulin) as well as EPAC play roles in activating RHO GTPases (66-68). This prompted us to ask if CDC42, RAC, and RHO participate in β-AR-induced ER-Mito contact formation.

To address this question, we investigated if inhibiting the activity of CDC42, RAC, or RHO, would alter the level of isoproterenol-induced split-Rluc reassembly. First, the CDC42 inhibitor ZCL 278 completely eradicated the effect of isoproterenol (Fig. 7C), supporting the role of CDC42 in isoproterenol-induced ER-Mito contacts likely by triggering actin polymerization. Next, the RAC inhibitor EHop 016 also reduced the level of split-Rluc reassembly when treated with or without isoproterenol (Fig. 7D, left). Its inhibitory effect, however, appears to be independent of blocking isoproterenol response, considering that the fold increase by isoproterenol over DMSO was in fact higher in EHop 016 treated cells when compared to vehicle treated ones (Fig. 7D, right). Finally, when RHO activity was inhibited by rhosin

(which binds directly to Rho GEF and thereby prevents RHO interaction with GEF), no changes in isoproterenol response was detected (Fig. 7E), indicating that RHO activity is not required.

Taken together, we conclude that actin polymerization triggered by CDC42 is a downstream event that is required to facilitate ER-Mito coupling, in response to β-AR signaling. We propose that EPAC activation via $G_{\alpha s}$/AC/cAMP pathway, and cytosolic Ca^{2+} increase under the influence of $G_{\alpha q}$/PLC/IP3 pathway, could be responsible for CDC42 activation (see Fig. 8), although further studies are certainly warranted.

Discussion

Communications between ER and mitochondria are crucial for many cellular functions. Although recent studies have focused on the molecular components of these contacts and suggested a few individual regulators (33), the regulatory signaling pathways of ER-Mito contacts remain largely unknown. In this study, we have made the novel discovery that select GPCRs, β-ARs in particular, are significant regulators of ER-Mito interactions. Upon ligand binding, β-ARs transduce the signal through $G_{\alpha s}$/AC/cAMP/EPAC and $G_{\alpha q}$/PLC/Ca^{2+} to induce physical contacts between the ER and mitochondria by stimulating actin polymerization. As a result, mitochondrial Ca^{2+} uptake is enhanced, thus activating mitochondrial matrix proteins to generate more ATPs (Fig. 8) (45, 49). Furthermore, revealing the ER-Mito contact enhancement as a new mechanism of action for β-AR agonists, our study highlights the strong potential of β-AR agonists as therapeutic options in diseases associated with disrupted ER-Mito contacts, as several β-AR agonists were already shown beneficial to Parkinson's disease prevention and treatment (36, 38, 69)

According to our data with $G_{\alpha s}$/cAMP pathway inhibitors, the isoproterenol-induced ER-Mito contact appears to be dependent on EPAC but not on PKA activation. In addition to the proposed potential mechanism (triggering actin polymerization through CDC42 activation) (Fig. 8), EPAC may exert its effect through a different mechanism. A recent study using mouse cardiomyocytes with genetic ablation of *Epac1* (*Epac1*$^{-/-}$) demonstrated that EPAC enhances ER-Mito interaction under stress by promoting the interaction between VDAC1, IP3R1, and GRP75, a well-established ER-Mito coupling complex (57). In wild type cells, when hypoxia/reoxygenation conditions were applied, ER-Mito contact was increased and a subsequent mitochondrial Ca^{2+} overload resulted in mitochondrial permeability transition pore (mPTP) opening, eventually leading to cell death. However, under the same conditions, Epac1$^{-/-}$ cells did not undergo cell death, due to no increase in ER-Mito interaction, thus no mitochondrial Ca^{2+} overload or mPTP opening (57). One can postulate that a similar increase in VDAC1/IP3R1/GRP75 interaction by EPAC could be an underlying mechanism of the isoproterenol-responsive ER-Mito contact formation, although further investigation is warranted.

In addition to the $G_{\alpha s}$/cAMP/EPAC pathway, $G_{\alpha q}$/PLC/Ca^{2+} pathway appears to be involved in isoproterenol-induced ER-Mito coupling. Given the weaker effect of chemical inhibitors of PLC than that of $G_{\alpha q}$, we postulate that the isoproterenol-induced cytosolic Ca^{2+} increase could be mediated not only by a direct activation of PLC/IP3, but possibly through an unknown pathway under β-AR/$G_{\alpha q}$ or through a crosstalk with $G_{\alpha s}$/cAMP/EPAC pathway. In this regard, it is interesting to note that a recent study showed EPAC agonist, 8-CPT-cAMP, promoted intracellular Ca^{2+} release, which was not through IP3 receptor, from sarcoplasmic reticulum (70).

Cytosolic Ca^{2+} increase may control other functions, in addition to its potential effect on actin polymerization. For instance, it might exert its effect through mitochondrial motility control, given that high cytosolic Ca^{2+} is known to arrest mitochondrial movement along the microtubule (71). Paused mitochondrial movement is thought to increase the likelihood of its interaction with ER (71). Consistent with this, when the split-Rluc activity was measured in the presence of nocodazole, an inhibitor of microtubule polymerization shown to block mitochondrial motility (71), ER-Mito contact was increased (Fig. S2C). Second, cytosolic Ca^{2+} surge might facilitate tethering complex formation directly. In agreement with this, E-Syt1 (extended synaptotagmin 1), an ER protein that participates in ER-plasma membrane (PM) tethering, has been shown to require cytosolic Ca^{2+} increases for its tethering functions (72). This raises the possibility that such tethering protein(s) may also exist in ER-Mito contacts. IP3 receptors (IP3Rs: IP3R1, 2 and 3) might be good candidates for such tethering proteins, given 1) the recent evidence on their structural roles in ER-Mito contact formation which were independent of their channel functions (73) and 2) the presence of Ca^{2+} binding sites on them (74). Finally, cytosolic Ca^{2+} rise might trigger activation of unknown regulatory molecules to enhance tethering between ER and mitochondria. In line with this, previous work has shown that Miro, a mitochondrial RHO GTPase (involved in mitochondrial transport) with two Ca^{2+} sensing EF-hand domains, enhances functional coupling between ER and mitochondria in a manner likely independent of mitochondrial transport (75). Our data in conjunction with this study suggest that Miro could be a good candidate modulator of ER-Mito contacts that responds to the increased cytosolic Ca^{2+}(75).

Our data with the MAPK pathway inhibitor PD0325901 (Fig. S2B) suggests that the activation of gene expression may not be required for isoproterenol-induced elevation in ER-Mito contacts and that the nature of drug-induced ER-Mito contacts is likely a short-term, immediate response to cellular demands. However, we cannot rule out the possibility that gene expression changes may play a role in ER-Mito contact modulation. Also, although we have not tested this pathway, it is possible that the non-canonical GPCR pathway via β-arrestin-2 may play a role in β-AR activated ER-Mito contact. In fact, low concentrations of β2-AR agonist (salmeterol) have been shown to act through the β-arrestin-2 pathway, not utilizing

cAMP/PKA or cAMP/EPAC pathway, when exerting its anti-inflammation effect in Parkinson's disease model (76).

Accumulating evidences indicate that ER-Mito contact dysfunction contributes to a variety of neurodegenerative diseases including Alzheimer's disease (AD), Parkinson's disease (PD), amyotrophic lateral sclerosis with associated fronto-temporal dementia (ALS/FTD), Charcot-Marie-Tooth (CMT) disease and hereditary spastic paraplegia (HSP) (19, 20, 77, 78). For example, disease-associated mutations in presenilin1 and 2 in AD (25, 26, 79, 80); α-synuclein (α-syn), DJ-1, PINK1 and parkin in PD (81-86); FUS, TDP43, SOD1 in ALS/FTD (32, 33); Mitofusin 2 in CMT (14); and REEP1 in HSP (23), have all shown to alter ER-Mito contacts, with evidence suggesting this change contributes to the neurodegeneration. It is interesting to speculate on the possibility that the drugs we have identified (that physically and functionally enhance ER-Mito contacts) represent potential therapeutics for conditions such as PD, ALS/FTD, and HSP, where reduced ER-Mito contacts have been implicated in pathogenesis. Accordingly, agonists to β2-AR have been shown to be beneficial in PD models, although the mechanism has been attributed to their anti-inflammatory activity (37, 87). Furthermore, salbutamol and metaproterenol (β2-AR agonists), both of which were also identified in our screen, reduce α-syn transcription levels, and salbutamol was associated with a reduced risk of developing PD in Norwegians and Israelis (36, 38). Although their efficacy was linked to α-syn transcription regulation (36) and anti-inflammation (76), our data indicate that these drugs might also exert therapeutic effects by increasing ER-Mito contacts as some PD associated insults appear to disrupt these contacts (85).

The results we present here also demonstrate that our split-Rluc reassembly assay can serve as a valid assay to screen for modulators of ER-Mito contacts. However, we recognize the likelihood of potential false negative hits in our screen due to its limitation with cell culture system (e.g., missing a repertoire of receptors or other necessary components) that might have resulted in biased screen results. In other words, if we have used a different cell line in our screen, we might have obtained a different set of compounds, although we expect they would be still within GPCR-associated compounds. For instance, if we had used Neuro2a cells that did not show isoproterenol response (Fig. S1C) probably due to the lack of β-AR expression (Table S4), other compounds targeting different GPCRs would have been identified. Another factor contributed to false negative hits in our screen would be its limitation related to potentially suboptimal conditions (e.g., concentration and stability) for some compounds. An example of such false negative compounds is GR79236, which is an A1-receptor selective agonist like CCPA and only differs by a hydroxyl-group on the N6-cyclopentyl-ring (CCPA has a chlorine in position 2), but showed substantially low activity compared to CCPA and did not make it to our positive hit list (Table S1).

While our current screen focused on an FDA-approved drug library, further screens with other compound libraries (identifying small molecules that could target ER-Mito contact sites directly) will likely

provide additional biologic insights into this important inter-organelle communication. Furthermore, ORF or siRNA library screens would be warranted to identify additional molecular machinery functioning for this contact. Finally, while our current screening system is most suitable for enhancer (or promoter) identification due to low basal level of split-Rluc activity, modification to our system could permit the screening for inhibitors of ER-Mito contacts in future studies.

Our screen results and subsequent exploration of drug mechanisms raise a significant point: the reason why β-AR agonists were identified as major ER-Mito contact modulators among other GPCRs is probably because β-ARs might be one of the most prominent GPCRs in H293T cells used in our drug screen (see Table S4). Alternatively, it is also possible that β-ARs might be the strongest regulator of ER-Mito contact among GPCRs. We think the first scenario is more plausible, given that $G_{\alpha s}$ CA or $G_{\alpha q}$ CA expression itself elevated ER-Mito contact (Fig. 5C, 6A) as well as ionomycin and CPA (Fig. 6F) which can enhance cytoplasmic Ca^{2+} level but are not components of β-AR pathway. Therefore, it appears that any GPCRs that can trigger cAMP/EPAC pathway activation or cytosolic Ca^{2+} increase may be able to modulate ER-Mito coupling, which means regulation of ER-Mito contact can be cell-type specific and different cells will respond differently to the same stress/stimuli depending on their GPCR availability. However, we cannot rule out the second scenario where β-AR specific pathway might be involved in ER-Mito contact regulation.

In summary, our data provide new insights into how changes in physiological demands in the cell can signal to induce changes in ER-Mito contacts that elicit physiological responses. Importantly, our study identifies a new mechanism of action for β2-AR agonists in PD prevention and treatment, and also offers potential therapeutic options for other conditions associated with disrupted ER-Mito contacts. When considering ER-Mito contact enhancement drugs for therapeutic options, however, it is important to recognize that both increased and decreased ER-Mito contacts can be detrimental. Therefore, careful titration of these drugs will be crucial. Furthermore, future studies will have to further address the detailed mechanisms of the GPCR pathway-regulated ER-Mito contacts and examine any distinctions, among different classes of GPCRs, in downstream pathways leading to ER-Mito contact modulation.

Experimental procedures

Plasmids and DNA constructs

Split-Rluc constructs in pcDNA3.1 (Mito-$Rluc^N$ and $Rluc^C$-ER) have been described previously (23). pCMV-mito-R-GECO1 (plasmid #46021), pAAV.CAG.GCaMP6s.WPRE.SV40 (plasmid #100844), and pAc-GFPC1-Sec61β (plasmid #15108) were obtained from Addgene (gift from Robert Campbell, Douglas Kim & GENIE Project, and Tom Rapoport, respectively) (42, 88, 89). CRE-luc2P (pGL4.29) was purchased from Promega (90, 91). Plasmids expressing Gs CA (Q227L), Gq CA (Q209L), Gi CA (Q205L),

and RAP1A DN (S17N) (56, 92, 93), were generated by cloning PCR-amplified cDNA fragments into pCAG-IRES-GFP (pCIG) vector (EcoRI/MluI). For the plasmid encoding β2-AR was generated by cloning PCR-amplified cDNA fragment into pCDH-EF1a-MCS-PGK-puro vector (EcoRI/NotI). For these cloning, HEK293T cDNAs, as a template, and specific primer sets including the ones containing mutations (see Table S6 for primer sequences) were used for PCR. All cDNAs were confirmed by sequencing.

Compounds and chemical reagents

We used NIH Clinical Collections 1 and 2 (NCC) (Evotec, San Francisco, CA) containing 720 FDA approved drugs dissolved in 100% DMSO at a concentration of 10 mM, for screening (note: the original list contains 727 drugs but 7 of them are duplicated). All drugs were used at 1 μM final concentration. The target pathway(s) of the members of this collection was manually curated from the information available in the PubChem portal (http://pubchem.ncbi.nlm.nih.gov/). Of note, NCC library contains 331 (46% of the 720 drugs) annotated drugs associated with GPCR pathways and 59 (18% of 331) drugs among these GPCR-associated drugs target ARs, according to our manual curation (Table S2).

For post-screen experiments, the chemical reagents were used as following: isoproterenol (1747, Tocris, 1μM), sotalol (0952, Tocris, 250 μM), actinomycin D (A9415, Sigma-Aldrich, 0.8 μM), CCPA (119136, Sigma-Aldrich, 1μM), prostaglandin E1 (P5515, Sigma-Aldrich, 1μM), ESI 09 (4773, Tocris, 5 μM), cAMPS-Rp (13371, Tocris, 10 μM), H89 (2910, Tocris, 10 μM), PD0325901 (04-0006, Reprocell, 1 μM), histamine (H7250, Sigma-Aldrich, 100 μM), ionomycin (1704, Tocris, 1 μM), and cyclopiazonic acid (CPA) (C1530, Sigma-Aldrich, 10 μM), thapsigargin (T9033, Sigma-Aldrich, 0.1-10 μM), ebselen (5245, Tocris, , 50 μM), edelfosine (3022, Tocris, 40 μM), U73122 (1268, Tocris, 5 μM), latrunculin (ab144290, Abcam, 1 μM), ZCL278 (4794, Tocris, 25 μM), EHop016 (6248, Tocris, 12.5 μM), rhosin (5003, Tocris, 25 μM), and nocodazole (S2775, Selleck Chemicals, 1, 4, and 10 ng/ml). For DMSO used as controls, the final concentration was decided according to the experimental drug's final concentration (e.g., 0.01% DMSO was used as a control, when other drugs (in 100 % DMSO) were used 1:10000 dilution).

Cell culture and transfection

HEK293T, HeLa, C2C12, and Neuro2a cells were maintained in DMEM (Thermo Fisher Scientific) with 10% (HEK293T, HeLa, Neuro2a) or 15% (C2C12) FBS (Thermo Fisher Scientific) in a humidified incubator at 37°C with 5% CO_2. For transfection with split-Rluc constructs, HEK293T cells (4 x 10^5 /well) were plated in a 12-well culture plate to obtain 75-80% confluency. After overnight culture, cells were transfected with indicated DNA constructs (400 ng each) using polyethylenimine (PEI; Polysciences, Eppelheim, Germany) as previously described (23, 34).

Split-Renilla luciferase (split-Rluc) reassembly assay

HEK293T cells were transfected with split-Rluc reporter plasmids (Mito-Rluc^{N} and Rluc^{C}-ER) in 12 well plates as described above. Four (all other experiments except for the screen) to six (for the screen) hours after transfection, cells were dissociated and re-plated into a 96-well plate (15,000 cells/well in 100 µl; white-wall plate, product no. 3610, Corning) coated with poly-D-lysine (50 µg/mL) and cultured overnight. Twenty-four hours post-transfection, live cell substrate, EnduRen (30 µM, Promega), was added to the culture media and incubated for 2-5 hours. For drug treatment, indicated drug(s) was added together with EnduRen. For the screen, the drugs (including isoproterenol) were treated for 5 hours; for subsequent split-Rluc assays, the cells were treated with isoproterenol for 2-4 hours. We have used different batches of HEK293T cells for the initial screen vs the subsequent experiments. Luminescence was measured by a POLARstar Omega microplate reader (BMG LABTECH, Ortenberg, Germany).

Library screen

HEK293T cells cultured in a 100 mm dish for 16 hours (with 75-80% confluency) were transfected with split-Rluc constructs (5 µg each). Six hours after transfection, cells were dissociated and plated onto 96-well plate (15,000 cells/well in 100 µl; white-wall plate, product no. 3610, Corning) coated with poly-D-lysine (50 µg/mL) and cultured overnight. Twenty-four hours post-transfection, 1 µM of each compound (final concentration) was added to each well together with Enduren (30 µM, Promega). Plates were incubated at 37°C with 5% CO_2 for 5 hours or longer and then luciferase activity (luminescence) was measured by a POLARstar Omega microplate reader (BMG LABTECH, Ortenberg, Germany). The initial screen was carried out only once. The split-Rluc activity of each drug was normalized by quantile normalization (39) using R statistical software (version 4.0). After normalization, the average and the standard deviation (SD) of the control (DMSO treatment) were calculated. Hits were picked using the cut-off value of three times of SD (3SD) higher than the average of the control, and further tested for their activity with split-Rluc assay. Only the compounds that showed consistently significant increase than DMSO were called as 'confirmed hits.' For drug enrichment analysis, we employed the over representation analysis (94). False discovery rate (FDR) was calculated by R software. Circular packaging dendrogram were created using R version 4.0.0 with packages 'ggraph', 'igraph, 'tidyverse' and 'RcolorBrewer'.

Proximity labeling assay (PLA)

HeLa cells were transfected with SEC61-GFP expression vector (100ng) in 8 well chamber slide (Millipore Sigma, Millicell EZ SLIDE) and, 16 hours post-transfection, treated with control (DMSO) or

indicated drugs for 5 hours. Cells were fixed with 4% paraformaldehyde for 15 min and permeabilized with 0.5% Triton X-100 for 5min. Proximity ligation assay (PLA) was performed according to the manufacturer's recommendation (Duolink™ In Situ Red Starter Kit Mouse/Rabbit, Sigma-Aldrich). HeLa cells were chosen over HEK293 cells for all PLAs in this study, given their relatively flat shape, which makes them more suitable for image analyses. Primary antibodies against GFP (ab13970 from chicken, Abcam) and Tom20 (sc-17764 from mouse, Santa Cruz Biotechnology) were used at 1:500 dilution each. After mounting, the images were captured by Zeiss Observer Z1 inverted microscope equipped with a Hamamatsu ORCA-Flash4.0 camera using Zeiss Zen Pro software. The image was analyzed in ImageJ with Maxima function. Number of PLA fluorescent puncta per cell was counted and averaged across multiple cells. For analyses, all PLA studies were internally compared.

Transmission Electron Microscopy (TEM)

HEK293T cells cultured in 100 mm dish with 90% confluency were treated with DMSO or isoproterenol for 30 min in the 37°C incubator with 5% CO_2. These monolayers of cells were fixed in the culture dish with glutaraldehyde/paraformaldehyde mixture (half-strength Karnovsky's fixative: 2g/dL paraformaldehyde, 2.5g/dL glutaraldehyde in 0.1M cacodylate buffer) (95) and post-fixed in 2% aqueous OsO_4 in 0.2M S-collidine buffer, pH 7.4. The monolayers were scrapped off the plastic dish with a rubber spatula, pelleted in a micro-centrifuge, dehydrated in graded ethanol solutions, transitioned into propylene oxide, and infiltrated and embedded in epoxy resin (Poly-Bed 812; Polysciences, Inc.; Warrington PA). One-micron thick sections were cut on an ultra-microtome and stained on the glass slide with 1g/dL toluidine blue in 1g/dL aqueous borax. Thin sections were mounted on 200 mesh copper grids and stained with saturated solution of uranyl acetate and 0.4g/dL alkaline lead citrate (96, 97). The stained grids were examined on a Jeol JEM-100CX electron microscope equipped with a digital camera. With randomly selected EM images, the distance between the outer mitochondrial membrane (OMM) and ER membrane was measured. If the distance (measured in Image J) was within 25 nm, it was counted as 'contact', whereas if it was greater than 25 nm, 'no contact'. The number of mitochondria with ER contact was counted and its percentage over the total number of mitochondria was calculated.

Calcium level measurement

To monitor the mitochondrial calcium dynamics, mito-R-GECO1 construct (100 ng each) was transfected into HeLa cells plated in the 8 well chamber slide (Nunc, Lab-Tek II). Sixteen hours after transfection, the cells were treated with DMSO or indicated drugs for 4 hours and were imaged on Zeiss Observer Z1 inverted microscope equipped with a Zeiss incubator system and a Hamamatsu ORCA-Flash4.0 camera.

Images were acquired using Zeiss Zen Pro software, every 2.5 sec for a duration of 5 min. Approximately 7.5 sec after the start of the experiment, histamine (100 μM) was superfused over transfected cells. For excitation of mito-R-GECO1, 535/40 nm filter was used; the emission filter was 624/40 nm. The boundary of each cell was set as ROIs (region of interest) and selected based on the presence of R-GECO1 fluorescent signal. $\Delta F/F_0$ was calculated as $(F-F_0)/F_0$, where F is fluorescence intensity of indicated fluorophore and F_0 is the baseline fluorescence intensity averaged over a 2.5-s period (during the control period) immediately before the start of histamine stimulation. The mitochondrial Ca^{2+} uptake rate was calculated as $(\Delta F/F_0)/\Delta t$ (R-GECO1) (from 7.5 to 12.5 sec) as described previously (98).

Mitochondrial transmembrane potential measurements

Mitochondrial membrane potential (Ψ_{mit}) was measured by tetramethyl rhodamine methyl ester (TMRM) fluorescent dye (I34361, Thermo Fisher Scientific). HeLa cells were loaded with 10 nM TMRM for 30 min at RT and then treated with DMSO or isoproterenol for 1 hour. TMRM fluorescence was imaged using an inverted microscope Zeiss Observer Z1 inverted microscope equipped with a Hamamatsu ORCA-Flash4.0 camera using Zeiss Zen Pro software, and analyzed in Image J.

GPCR expression level analysis

Publicly available gene expression profiles of the three cell lines (HEK293T, HeLa, and Neuro2a) (Table S4) were analyzed by DEseq2 (99). The raw seq-data were downloaded from Geo Dataset server with each GEO set access number (HEK293T, GSE99249; Hela, GSE143517; Neuro2a, GSE60241). Alignment of read mRNA-sequence to genome was performed with Salmon (100). The tximport (101) was utilized to calculate counts per gene. The base mean of each GPCR is computed by DEseq2 (99).

Statistical analysis

All statistical analyses were performed using GraphPad Prism (version 8.4.2) or R (version 4.0.0). To determine whether differences between two data sets are statistically significant, two-tailed paired or unpaired *t*-test was used if the data passed normality test; non-parametric test (Mann Whitney test) was used if failed normality test. When more than two data sets were compared, 1- or 2- way ANOVA test was used if passed normality test; other tests recommended by Prism software (e.g., Kruskal-Wallis test, Brown-Forsythe ANOVA test, Welch's ANOVA test) were used if failed normality test. For comparisons of multiple samples following these tests, Dunn's test, Dunnett's test, or Sidak's test was used. For contingency table, Chi-square test (and Fisher's exact test) was used. The details of all statistical tests including the exact *p*-values and sample numbers (*n*) are listed in the figure legends or directly in the graphs.

P values ≤ 0.05 were considered statistically significant. When fold changes were used, all data were normalized to control (e.g., DMSO). All bar graphs are plotted as mean ± standard deviation (SD) and individual data points are marked with dots. Concentration responsive curves are plotted as mean ± 95% confidence interval (curve fit with non-linear regression). All scattered plots are marked with individual data points and mean ± standard deviation (SD).

Acknowledgement

This work was supported by the National Institute of Neurological Disorders and Stroke (R01NS100007) and Dana-Farber Cancer Institute microgrant (#120205). The authors are grateful to Dr Jeffrey A. Golden and his lab members (Brigham and Women's Hospital/Harvard Medical School) for their support on this study as well as critical review of the manuscript, to Drs Sean E. Lawler and Michal Oscar Nowicki (Brigham and Women's Hospital/Harvard Medical School) for sharing their reagents and equipment, to Amanda Frischmann for her assistance on compound list curating process, and to Dr Wei Wang (Brigham and Women's Hospital/Dana-Farber Cancer Institute/Harvard Medical School) for her help with statistical analyses, supported by the Harvard Catalyst|The Harvard Clinical and Translational Science Center (National Center for Advancing Translational Sciences, NIH award UL 1TR002541) and financial contributions from Harvard University and its affiliated academic healthcare centers. The content is solely the responsibility of the authors and does not necessarily represent the official views of Harvard Catalyst, Harvard University and its affiliated academic healthcare centers, or the NIH.

Conflict of interest

The authors declare that they have no conflicts of interest with the contents of this article.

The content is solely the responsibility of the authors and does not necessarily represent the official views of the National Institutes of Health.

References

1. Rowland, A. A., and Voeltz, G. K. (2012) Endoplasmic reticulum-mitochondria contacts: function of the junction. *Nat Rev Mol Cell Biol*. **13**, 607–625

2. Csordás, G., Weaver, D., and Hajnóczky, G. (2018) Endoplasmic reticulum-mitochondrial contactology: structure and signaling Functions. *Trends in Cell Biology*. **28**, 523–540

3. Scorrano, L., De Matteis, M. A., Emr, S., Giordano, F., Hajnóczky, G., Kornmann, B., Lackner, L. L., Levine, T. P., Pellegrini, L., Reinisch, K., Rizzuto, R., Simmen, T., Stenmark, H., Ungermann, C., and Schuldiner, M. (2019) Coming together to define membrane contact sites. *Nature Communications*. **10**, 1287

4. Kornmann, B., Currie, E., Collins, S. R., Schuldiner, M., Nunnari, J., Weissman, J. S., and Walter, P. (2009) An ER-mitochondria tethering complex revealed by a synthetic biology screen. *Science*. **325**, 477–481

5. Lang, A., Peter, A. T. J., and Kornmann, B. (2015) ER–mitochondria contact sites in yeast: beyond the myths of ERMES. *Current Opinion in Cell Biology*. **35**, 7–12

6. Eisenberg-Bord, M., Shai, N., Schuldiner, M., and Bohnert, M. (2016) A tether is a tether is a tether: Tethering at membrane contact sites. *Dev. Cell*. **39**, 395–409

7. Kornmann, B. (2013) The molecular hug between the ER and the mitochondria. *Current Opinion in Cell Biology*. **25**, 443–448

8. Lee, S., and Min, K.-T. (2018) The interface between ER and mitochondria: Molecular compositions and functions. *Mol. Cells*. **41**, 1000–1007

9. Vance, J. E. (2014) MAM (mitochondria-associated membranes) in mammalian cells: lipids and beyond. *Biochim. Biophys. Acta*. **1841**, 595–609

10. Vance, J. E. (1990) Phospholipid synthesis in a membrane fraction associated with mitochondria. *J Biol Chem*. **265**, 7248–7256

11. Rizzuto, R., Brini, M., Murgia, M., and Pozzan, T. (1993) Microdomains with high Ca2+ close to IP3-sensitive channels that are sensed by neighboring mitochondria. *Science*. **262**, 744–747

12. Rizzuto, R., Pinton, P., Carrington, W., Fay, F. S., Fogarty, K. E., Lifshitz, L. M., Tuft, R. A., and Pozzan, T. (1998) Close contacts with the endoplasmic reticulum as determinants of mitochondrial Ca2+ responses. *Science*. **280**, 1763–1766

13. Booth, D. M., Enyedi, B., Geiszt, M., Várnai, P., and Hajnóczky, G. (2016) Redox Nanodomains Are Induced by and Control Calcium Signaling at the ER-Mitochondrial Interface. *Mol. Cell*. **63**, 240–248

14. de Brito, O. M., and Scorrano, L. (2008) Mitofusin 2 tethers endoplasmic reticulum to mitochondria. *Nature*. **456**, 605–610

15. Friedman, J. R., Lackner, L. L., West, M., DiBenedetto, J. R., Nunnari, J., and Voeltz, G. K. (2011) ER tubules mark sites of mitochondrial division. *Science*. **334**, 358–362

16. Hamasaki, M., Furuta, N., Matsuda, A., Nezu, A., Yamamoto, A., Fujita, N., Oomori, H., Noda, T., Haraguchi, T., Hiraoka, Y., Amano, A., and Yoshimori, T. (2013) Autophagosomes form at ER-mitochondria contact sites. *Nature*. **495**, 389–393

17. Böckler, S., and Westermann, B. (2014) Mitochondrial ER contacts are crucial for mitophagy in yeast. *Dev. Cell*. **28**, 450–458

18. Simmen, T., Aslan, J. E., Blagoveshchenskaya, A. D., Thomas, L., Wan, L., Xiang, Y., Feliciangeli, S. F., Hung, C.-H., Crump, C. M., and Thomas, G. (2005) PACS-2 controls endoplasmic reticulum-mitochondria communication and Bid-mediated apoptosis. *EMBO J*. **24**, 717–729

19. Paillusson, S., Stoica, R., Gomez-Suaga, P., Lau, D. H. W., Mueller, S., Miller, T., and Miller, C. C. J. (2016) There's something wrong with my MAM; the ER-mitochondria axis and neurodegenerative diseases. *Trends Neurosci*. **39**, 146–157

20. Moltedo, O., Remondelli, P., and Amodio, G. (2019) The mitochondria-endoplasmic reticulum contacts and their critical role in aging and age-associated diseases. *Front. Cell Dev. Biol.* **7**, 172

21. Rieusset, J. (2018) The role of endoplasmic reticulum-mitochondria contact sites in the control of glucose homeostasis: an update. *Cell Death and Disease*. **9**, 388

22. Doghman Bouguerra, M., and Lalli, E. (2019) ER-mitochondria interactions: Both strength and weakness within cancer cells. *Biochim Biophys Acta Mol Cell Res*. **1866**, 650–662

23. Lim, Y., Cho, I.-T., Schoel, L. J., Cho, G., and Golden, J. A. (2015) Hereditary spastic paraplegia-linked REEP1 modulates endoplasmic reticulum/mitochondria contacts. *Ann Neurol*. **78**, 679–696

24. Tambini, M. D., Pera, M., Kanter, E., Yang, H., Guardia-Laguarta, C., Holtzman, D., Sulzer, D., Area-Gomez, E., and Schon, E. A. (2016) ApoE4 upregulates the activity of mitochondria-associated ER membranes. *EMBO Rep.* **17**, 27–36

25. Area-Gomez, E., del Carmen Lara Castillo, M., Tambini, M. D., Guardia-Laguarta, C., de Groof, A. J. C., Madra, M., Ikenouchi, J., Umeda, M., Bird, T. D., Sturley, S. L., and Schon, E. A. (2012) Upregulated function of mitochondria-associated ER membranes in Alzheimer disease. *The EMBO Journal*. **31**, 4106–4123

26. Hedskog, L., Pinho, C. M., Filadi, R., Rönnbäck, A., Hertwig, L., Wiehager, B., Larssen, P., Gellhaar, S., Sandebring, A., Westerlund, M., Graff, C., Winblad, B., Galter, D., Behbahani, H., Pizzo, P., Glaser, E., and Ankarcrona, M. (2013) Modulation of the endoplasmic reticulum-mitochondria interface in Alzheimer's disease and related models. *Proceedings of the National Academy of Sciences*. **110**, 7916–7921

27. Zampese, E., Fasolato, C., Kipanyula, M. J., Bortolozzi, M., Pozzan, T., and Pizzo, P. (2011) Presenilin 2 modulates endoplasmic reticulum (ER)-mitochondria interactions and Ca2+ cross-talk. *Proceedings of the National Academy of Sciences*. **108**, 2777–2782

28. Tepikin, A. V. (2018) Mitochondrial junctions with cellular organelles: Ca2+ signalling perspective. *Pflugers Arch - Eur J Physiol*. **470**, 1181–1192

29. Stoica, R., De Vos, K. J., Paillusson, S., Mueller, S., Sancho, R. M., Lau, K.-F., Vizcay-Barrena, G., Lin, W.-L., Xu, Y.-F., Lewis, J., Dickson, D. W., Petrucelli, L., Mitchell, J. C., Shaw, C. E., and Miller, C. C. J. (2014) ER-mitochondria associations are regulated by the VAPB-PTPIP51 interaction and are disrupted by ALS/FTD-associated TDP-43. *Nature Communications*. **5**, 3996

30. Stoica, R., Paillusson, S., Gomez-Suaga, P., Mitchell, J. C., Lau, D. H., Gray, E. H., Sancho, R. M., Vizcay-Barrena, G., De Vos, K. J., Shaw, C. E., Hanger, D. P., Noble, W., and Miller, C. C. (2016) ALS/FTD-associated FUS activates GSK-3β to disrupt the VAPB-PTPIP51 interaction and ER-mitochondria associations. *EMBO Rep.* **17**, 1326–1342

31. Watanabe, S., Ilieva, H., Tamada, H., Nomura, H., Komine, O., Endo, F., Jin, S., Mancias, P., Kiyama, H., and Yamanaka, K. (2016) Mitochondria-associated membrane collapse is a common pathomechanism in SIGMAR1- and SOD1-linked ALS. *EMBO Mol Med*. **8**, 1421–1437

32. Lau, D. H. W., Hartopp, N., Welsh, N. J., Mueller, S., Glennon, E. B., Mórotz, G. M., Annibali, A., Gomez-Suaga, P., Stoica, R., Paillusson, S., and Miller, C. C. J. (2018) Disruption of ER-mitochondria signalling in fronto-temporal dementia and related amyotrophic lateral sclerosis. *Cell Death and Disease*. **9**, 327

33. Le Masson, G., Przedborski, S., and Abbott, L. F. (2014) A computational model of motor neuron degeneration. *Neuron*. **83**, 975–988

34. Cho, I.-T., Adelmant, G., Lim, Y., Marto, J. A., Cho, G., and Golden, J. A. (2017) Ascorbate peroxidase proximity labeling coupled with biochemical fractionation identifies promoters of endoplasmic reticulum-mitochondrial contacts. *J Biol Chem*. **292**, 16382–16392

35. Neumann, E., Khawaja, K., and Müller-Ladner, U. (2014) G protein-coupled receptors in rheumatology. *Nat Rev Rheumatol*. **10**, 429–436

36. Mittal, S., Bjørnevik, K., Im, D. S., Flierl, A., Dong, X., Locascio, J. J., Abo, K. M., Long, E., Jin, M., Xu, B., Xiang, Y. K., Rochet, J.-C., Engeland, A., Rizzu, P., Heutink, P., Bartels, T., Selkoe, D. J., Caldarone, B. J., Glicksman, M. A., Khurana, V., Schüle, B., Park, D. S., Riise, T., and Scherzer, C. R. (2017) β2-Adrenoreceptor is a regulator of the α-synuclein gene driving risk of Parkinson's disease. *Science*. **357**, 891–898

37. Peterson, L., Ismond, K. P., Chapman, E., and Flood, P. (2014) Potential benefits of therapeutic use of β2-adrenergic receptor agonists in neuroprotection and Parkinson's disease. *J Immunol Res*. **2014**, 103780

38. Gronich, N., Abernethy, D. R., Auriel, E., Lavi, I., Rennert, G., and Saliba, W. (2018) β2-adrenoceptor agonists and antagonists and risk of Parkinson's disease. *Mov Disord.* **33**, 1465–1471

39. Bolstad, B. M., Irizarry, R. A., Astrand, M., and Speed, T. P. (2003) A comparison of normalization methods for high density oligonucleotide array data based on variance and bias. *Bioinformatics*. **19**, 185–193

40. Söderberg, O., Gullberg, M., Jarvius, M., Ridderstråle, K., Leuchowius, K.-J., Jarvius, J., Wester, K., Hydbring, P., Bahram, F., Larsson, L.-G., and Landegren, U. (2006) Direct observation of individual endogenous protein complexes in situ by proximity ligation. *Nat Meth*. **3**, 995–1000

41. Giacomello, M., Drago, I., Bortolozzi, M., Scorzeto, M., Gianelle, A., Pizzo, P., and Pozzan, T. (2010) Ca2+ hot spots on the mitochondrial surface are generated by Ca2+ mobilization from stores, but not by activation of store-operated Ca2+ channels. *Mol. Cell*. **38**, 280–290

42. Wu, J., Liu, L., Matsuda, T., Zhao, Y., Rebane, A., Drobizhev, M., Chang, Y.-F., Araki, S., Arai, Y., March, K., Hughes, T. E., Sagou, K., Miyata, T., Nagai, T., Li, W.-H., and Campbell, R. E.

(2013) Improved orange and red Ca²± indicators and photophysical considerations for optogenetic applications. *ACS Chem Neurosci*. **4**, 963–972

43. Zhao, Y., Araki, S., Wu, J., Teramoto, T., Chang, Y.-F., Nakano, M., Abdelfattah, A. S., Fujiwara, M., Ishihara, T., Nagai, T., and Campbell, R. E. (2011) An expanded palette of genetically encoded Ca^{2+} indicators. *Science*. **333**, 1888–1891

44. Filadi, R., Leal, N. S., Schreiner, B., Rossi, A., Dentoni, G., Pinho, C. M., Wiehager, B., Cieri, D., Calì, T., Pizzo, P., and Ankarcrona, M. (2018) TOM70 sustains cell bioenergetics by promoting IP3R3-mediated ER to mitochondria Ca2+ transfer. *Curr Biol*. **28**, 369–382.e6

45. Bravo, R., Vicencio, J. M., Parra, V., Troncoso, R., Munoz, J. P., Bui, M., Quiroga, C., Rodriguez, A. E., Verdejo, H. E., Ferreira, J., Iglewski, M., Chiong, M., Simmen, T., Zorzano, A., Hill, J. A., Rothermel, B. A., Szabadkai, G., and Lavandero, S. (2011) Increased ER-mitochondrial coupling promotes mitochondrial respiration and bioenergetics during early phases of ER stress. *J Cell Sci*. **124**, 2143–2152

46. Cárdenas, C., Miller, R. A., Smith, I., Bui, T., Molgó, J., Müller, M., Vais, H., Cheung, K.-H., Yang, J., Parker, I., Thompson, C. B., Birnbaum, M. J., Hallows, K. R., and Foskett, J. K. (2010) Essential regulation of cell bioenergetics by constitutive InsP3 receptor Ca2+ transfer to mitochondria. *Cell*. **142**, 270–283

47. Balaban, R. S. (2009) The role of Ca(2+) signaling in the coordination of mitochondrial ATP production with cardiac work. *Biochim. Biophys. Acta*. **1787**, 1334–1341

48. Territo, P. R., Mootha, V. K., French, S. A., and Balaban, R. S. (2000) Ca(2+) activation of heart mitochondrial oxidative phosphorylation: role of the F(0)/F(1)-ATPase. *Am. J. Physiol., Cell Physiol.* **278**, C423–35

49. Denton, R. M. (2009) Regulation of mitochondrial dehydrogenases by calcium ions. *Biochim. Biophys. Acta*. **1787**, 1309–1316

50. Perry, C. G. R., Kane, D. A., Lanza, I. R., and Neufer, P. D. (2013) Methods for assessing mitochondrial function in diabetes. *Diabetes*. **62**, 1041–1053

51. Scaduto, R. C., and Grotyohann, L. W. (1999) Measurement of mitochondrial membrane potential using fluorescent rhodamine derivatives. *Biophysj*. **76**, 469–477

52. Inoue, A., Raimondi, F., Kadji, F. M. N., Singh, G., Kishi, T., Uwamizu, A., Ono, Y., Shinjo, Y., Ishida, S., Arang, N., Kawakami, K., Gutkind, J. S., Aoki, J., and Russell, R. B. (2019) Illuminating G-protein-coupling selectivity of GPCRs. *Cell*. **177**, 1933–1947.e25

53. Luttrell, L. M., Roudabush, F. L., Choy, E. W., Miller, W. E., Field, M. E., Pierce, K. L., and Lefkowitz, R. J. (2001) Activation and targeting of extracellular signal-regulated kinases by beta-arrestin scaffolds. *Proc Natl Acad Sci USA*. **98**, 2449–2454

54. Gutkind, J. S. (1998) The pathways connecting G protein-coupled receptors to the nucleus through divergent mitogen-activated protein kinase cascades. *J Biol Chem*. **273**, 1839–1842

55. Blaukat, A., Barac, A., Cross, M. J., Offermanns, S., and Dikic, I. (2000) G protein-coupled receptor-mediated mitogen-activated protein kinase activation through cooperation of Galpha(q) and Galpha(i) signals. *Mol Cell Biol*. **20**, 6837–6848

56. Huang, X.-P., Song, X., Wang, H.-Y., and Malbon, C. C. (2002) Targeted expression of activated Q227L G(alpha)(s) in vivo. *Am. J. Physiol., Cell Physiol.* **283**, C386–95

57. Fazal, L., Laudette, M., Paula-Gomes, S., Pons, S., Conte, C., Tortosa, F., Sicard, P., Sainte-Marie, Y., Bisserier, M., Lairez, O., Lucas, A., Roy, J., Ghaleh, B., Fauconnier, J., Mialet-Perez, J., and Lezoualc'H, F. (2017) Multifunctional mitochondrial epac1 controls myocardial cell death. *Circulation Research*. **120**, 645–657

58. Kuschak, M., Namasivayam, V., Rafehi, M., Voss, J. H., Garg, J., Schlegel, J. G., Abdelrahman, A., Kehraus, S., Reher, R., Küppers, J., Sylvester, K., Hinz, S., Matthey, M., Wenzel, D., Fleischmann, B. K., Pfeifer, A., Inoue, A., Gütschow, M., König, G. M., and Müller, C. E. (2020) Cell-permeable high-affinity tracers for Gq proteins provide structural insights, reveal distinct binding kinetics and identify small molecule inhibitors. *British Journal of Pharmacology*. **177**, 1898–1916

59. Azad, G. K., and Tomar, R. S. (2014) Ebselen, a promising antioxidant drug: mechanisms of action and targets of biological pathways. *Mol. Biol. Rep.* **41**, 4865–4879

60. Chakrabarti, R., Ji, W.-K., Stan, R. V., de Juan Sanz, J., Ryan, T. A., and Higgs, H. N. (2018) INF2-mediated actin polymerization at the ER stimulates mitochondrial calcium uptake, inner membrane constriction, and division. *J. Cell Biol.* **217**, 251–268

61. Plenge-Tellechea, F., Soler, F., and Fernandez-Belda, F. (1997) On the inhibition mechanism of sarcoplasmic or endoplasmic reticulum Ca2+-ATPases by cyclopiazonic acid. *J Biol Chem*. **272**, 2794–2800

62. Ji, W.-K., Chakrabarti, R., Fan, X., Schoenfeld, L., Strack, S., and Higgs, H. N. (2017) Receptor-mediated Drp1 oligomerization on endoplasmic reticulum. *J. Cell Biol.* **216**, 4123–4139

63. Shao, X., Li, Q., Mogilner, A., Bershadsky, A. D., and Shivashankar, G. V. (2015) Mechanical stimulation induces formin-dependent assembly of a perinuclear actin rim. *Proceedings of the National Academy of Sciences*. **112**, E2595–601

64. Hall, A. (1998) Rho GTPases and the actin cytoskeleton. *Science*. **279**, 509–514

65. Sinha, S., and Yang, W. (2008) Cellular signaling for activation of Rho GTPase Cdc42. *Cell. Signal.* **20**, 1927–1934

66. Momotani, K., and Somlyo, A. V. (2012) p63RhoGEF: a new switch for G(q)-mediated activation of smooth muscle. *Trends Cardiovasc. Med.* **22**, 122–127

67. van Unen, J., Yin, T., Wu, Y. I., Mastop, M., Gadella, T. W. J., and Goedhart, J. (2016) Kinetics of recruitment and allosteric activation of ARHGEF25 isoforms by the heterotrimeric G-protein Gαq. *Scientific Reports*. **6**, 36825

68. Jin, M., Guan, C.-B., Jiang, Y.-A., Chen, G., Zhao, C.-T., Cui, K., Song, Y.-Q., Wu, C.-P., Poo, M.-M., and Yuan, X.-B. (2005) Ca2+-dependent regulation of rho GTPases triggers turning of nerve growth cones. *J Neurosci*. **25**, 2338–2347

69. Peterson, L., Ismond, K. P., Chapman, E., and Flood, P. (2014) Potential benefits of therapeutic use of β2-adrenergic receptor agonists in neuroprotection and Parkinsonμs disease. *J Immunol Res*. **2014**, 103780

70. Cuíñas, A., García-Morales, V., Viña, D., Gil-Longo, J., and Campos-Toimil, M. (2016) Activation of PKA and Epac proteins by cyclic AMP depletes intracellular calcium stores and reduces calcium availability for vasoconstriction. *Life Sci.* **155**, 102–109

71. Yi, M., Weaver, D., and Hajnóczky, G. (2004) Control of mitochondrial motility and distribution by the calcium signal: a homeostatic circuit. *J. Cell Biol.* **167**, 661–672

72. Giordano, F., Saheki, Y., Idevall-Hagren, O., Colombo, S. F., Pirruccello, M., Milosevic, I., Gracheva, E. O., Bagriantsev, S. N., Borgese, N., and De Camilli, P. (2013) PI(4,5)P(2)-dependent and Ca(2+)-regulated ER-PM interactions mediated by the extended synaptotagmins. *Cell*. **153**, 1494–1509

73. Bartok, A., Weaver, D., Golenár, T., Nichtova, Z., Katona, M., Bánsághi, S., Alzayady, K. J., Thomas, V. K., Ando, H., Mikoshiba, K., Joseph, S. K., Yule, D. I., Csordás, G., and Hajnóczky, G. (2019) IP3 receptor isoforms differently regulate ER-mitochondrial contacts and local calcium transfer. *Nature Communications*. **10**, 3726

74. Taylor, C. W., and Tovey, S. C. (2010) IP(3) receptors: toward understanding their activation. *Cold Spring Harbor Perspectives in Biology*. **2**, a004010

75. Lee, S., Lee, K.-S., Huh, S., Liu, S., Lee, D.-Y., Hong, S. H., Yu, K., and Lu, B. (2016) Polo Kinase Phosphorylates Miro to Control ER-Mitochondria Contact Sites and Mitochondrial Ca(2+) Homeostasis in Neural Stem Cell Development. **37**, 174–189

76. Qian, L., Wu, H.-M., Chen, S.-H., Zhang, D., Ali, S. F., Peterson, L., Wilson, B., Lu, R.-B., Hong, J.-S., and Flood, P. M. (2011) β2-adrenergic receptor activation prevents rodent dopaminergic neurotoxicity by inhibiting microglia via a novel signaling pathway. *J. Immunol.* **186**, 4443–4454

77. Joshi, A. U., Kornfeld, O. S., and Mochly-Rosen, D. (2016) The entangled ER-mitochondrial axis as a potential therapeutic strategy in neurodegeneration: A tangled duo unchained. *Cell Calcium*. **60**, 218–234

78. Krols, M., van Isterdael, G., Asselbergh, B., Kremer, A., Lippens, S., Timmerman, V., and Janssens, S. (2016) Mitochondria-associated membranes as hubs for neurodegeneration. *Acta Neuropathol*. **131**, 505–523

79. Schon, E. A., and Area-Gomez, E. (2013) Mitochondria-associated ER membranes in Alzheimer disease. *Mol Cell Neurosci*. **55**, 26–36

80. Filadi, R., Greotti, E., Turacchio, G., Luini, A., Pozzan, T., and Pizzo, P. (2016) Presenilin 2 Modulates Endoplasmic Reticulum-Mitochondria Coupling by Tuning the Antagonistic Effect of Mitofusin 2. *CellReports*. **15**, 2226–2238

81. Paillusson, S., Gomez-Suaga, P., Stoica, R., Little, D., Gissen, P., Devine, M. J., Noble, W., Hanger, D. P., and Miller, C. C. J. (2017) α-Synuclein binds to the ER-mitochondria tethering protein VAPB to disrupt Ca2+ homeostasis and mitochondrial ATP production. *Acta Neuropathol*. **134**, 129–149

82. Gautier, C. A., Erpapazoglou, Z., Mouton-Liger, F., Muriel, M.-P., Cormier, F., Bigou, S., Duffaure, S., Girard, M., Foret, B., Iannielli, A., Broccoli, V., Dalle, C., Bohl, D., Michel, P. P., Corvol, J.-C., Brice, A., and Corti, O. (2016) The endoplasmic reticulum-mitochondria interface is perturbed in PARK2 knockout mice and patients with PARK2 mutations. *Hum Mol Genet*. **25**, 2972–2984

83. Calì, T., Ottolini, D., Negro, A., and Brini, M. (2012) α-Synuclein controls mitochondrial calcium homeostasis by enhancing endoplasmic reticulum-mitochondria interactions. *J Biol Chem*. **287**, 17914–17929

84. Gelmetti, V., De Rosa, P., Torosantucci, L., Marini, E. S., Romagnoli, A., Di Rienzo, M., Arena, G., Vignone, D., Fimia, G. M., and Valente, E. M. (2017) PINK1 and BECN1 relocalize at mitochondria-associated membranes during mitophagy and promote ER-mitochondria tethering and autophagosome formation. *Autophagy*. **13**, 654–669

85. Barazzuol, L., Giamogante, F., Brini, M., and Calì, T. (2020) PINK1/Parkin mediated mitophagy, Ca2+ signalling, and ER-mitochondria contacts in Parkinson's disease. *IJMS*. 10.3390/ijms21051772

86. Ottolini, D., Calì, T., Negro, A., and Brini, M. (2013) The Parkinson disease-related protein DJ-1 counteracts mitochondrial impairment induced by the tumour suppressor protein p53 by enhancing endoplasmic reticulum-mitochondria tethering. *Hum Mol Genet*. **22**, 2152–2168

87. Magistrelli, L., and Comi, C. (2020) Beta2-adrenoceptor agonists in Parkinson's disease and other synucleinopathies. *J Neuroimmune Pharmacol*. **15**, 74–81

88. Chen, T.-W., Wardill, T. J., Sun, Y., Pulver, S. R., Renninger, S. L., Baohan, A., Schreiter, E. R., Kerr, R. A., Orger, M. B., Jayaraman, V., Looger, L. L., Svoboda, K., and Kim, D. S. (2013) Ultrasensitive fluorescent proteins for imaging neuronal activity. *Nature*. **499**, 295–300

89. Voeltz, G. K., Prinz, W. A., Shibata, Y., Rist, J. M., and Rapoport, T. A. (2006) A class of membrane proteins shaping the tubular endoplasmic reticulum. *Cell*. **124**, 573–586

90. Clipstone, N. A., and Crabtree, G. R. (1992) Identification of calcineurin as a key signalling enzyme in T-lymphocyte activation. *Nature*. **357**, 695–697

91. Lyakh, L., Ghosh, P., and Rice, N. R. (1997) Expression of NFAT-family proteins in normal human T cells. *Mol Cell Biol*. **17**, 2475–2484

92. Murga, C., Laguinge, L., Wetzker, R., Cuadrado, A., and Gutkind, J. S. (1998) Activation of Akt/protein kinase B by G protein-coupled receptors. A role for alpha and beta gamma subunits of heterotrimeric G proteins acting through phosphatidylinositol-3-OH kinasegamma. *J Biol Chem*. **273**, 19080–19085

93. Dupuy, A. G., LHoste, S., Cherfils, J., Camonis, J., Gaudriault, G., and Gunzburg, J. de (2020) Novel Rap1 dominant-negative mutants interfere selectively with C3G and Epac. *Oncogene*. **24**, 4509–4520

94. Boyle, E. I., Weng, S., Gollub, J., Jin, H., Botstein, D., Cherry, J. M., and Sherlock, G. (2004) GO::TermFinder--open source software for accessing Gene Ontology information and finding significantly enriched Gene Ontology terms associated with a list of genes. *Bioinformatics*. **20**, 3710–3715

95. Karnovsky, M. J. (1965) A formaldehyde-glutaraldehyde fixative of high osmolality for use in electron microscopy. J. Cell Biol. 27:137-8A, 1965. *J. Cell Biol.*

96. Venable, J.H. & Coggeshall, R. (1965) A simplified lead citrate stain for use in electron microscopty. *J. Cell Biol.* **25**, 407–408

97. Reynolds, E.S. (1963) The use of lead citrate at high pH as an electron-opaque stain in electron microscopy. *J. Cell Biol.* **17**, 208–212

98. Fülöp, L., Szanda, G., Enyedi, B., Várnai, P., and Spät, A. (2011) The effect of OPA1 on mitochondrial Ca^{2+} signaling. *PLoS ONE*. **6**, e25199

99. Love, M. I., Huber, W., and Anders, S. (2014) Moderated estimation of fold change and dispersion for RNA-seq data with DESeq2. *Genome Biol*. **15**, 550

100. Patro, R., Duggal, G., Love, M. I., Irizarry, R. A., and Kingsford, C. (2017) Salmon provides fast and bias-aware quantification of transcript expression. *Nat Meth*. **14**, 417–419

101. Soneson, C., Love, M. I., and Robinson, M. D. (2015) Differential analyses for RNA-seq: transcript-level estimates improve gene-level inferences. *F1000Res*. **4**, 1521

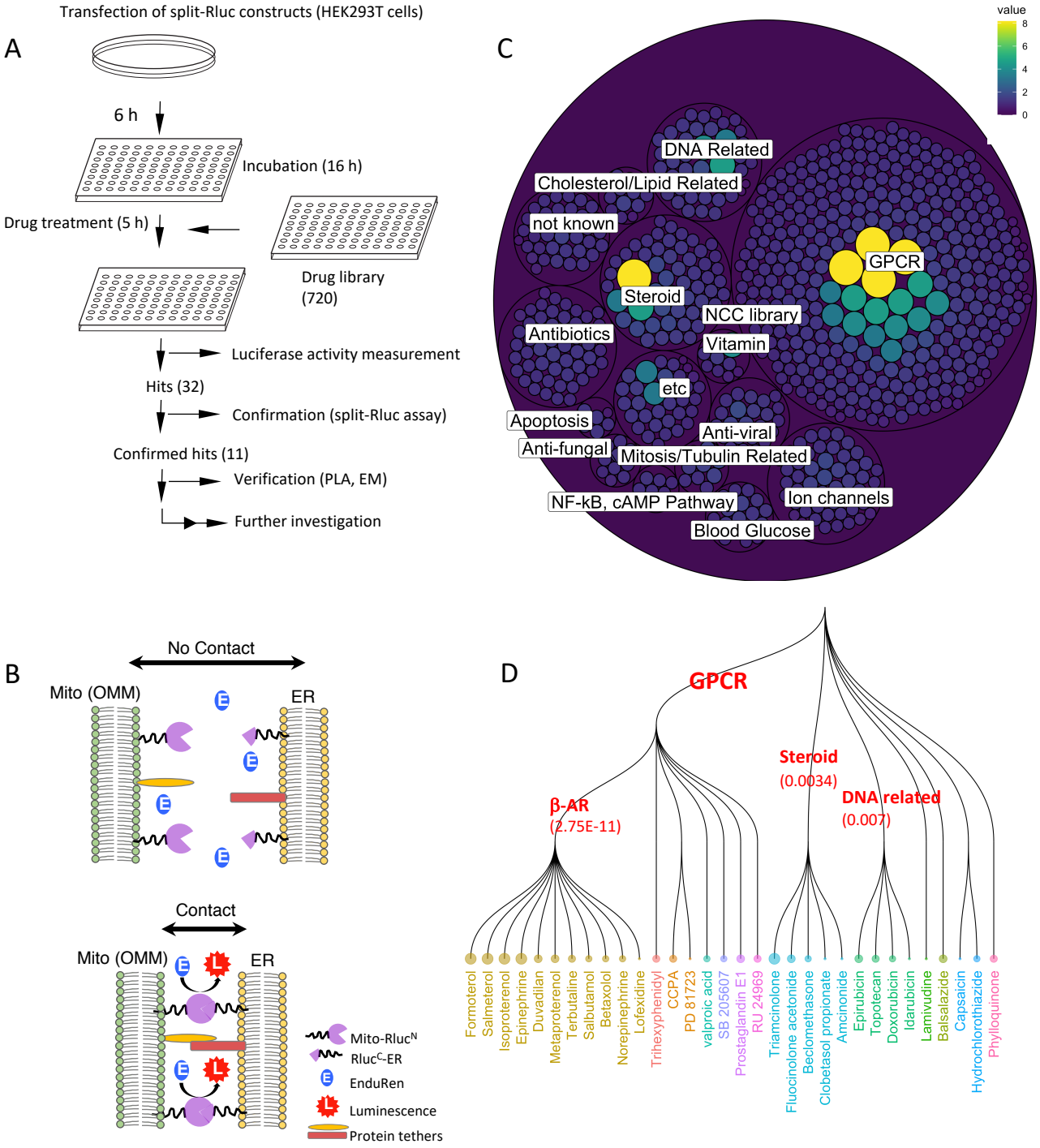

Figure 1. Drug screening with split-Rluc assay system. *A,* *A* schematic showing drug screening workflow. EM, electron microscopy; NCC, NIH Clinical Collection; PLA, proximity ligase assay; Rluc, *Renilla* luciferase. ***B,*** A schematic of split-Rluc assay and its components (adapted from ref. 34). ER, endoplasmic reticulum membrane; Mito, mitochondria; Mito-Rluc^{N}, N-terminal half of the Rluc with mitochondria targeting sequence; OMM, outer mitochondrial membrane; Rluc^{C}-ER, C-terminal half of the Rluc with ER targeting sequence. ***C,*** Initial screen results depicted with circular packaging of library drugs grouped into their predicted target pathway (each circle: each drug; circle size: normalized split-Rluc activity). Green to yellow circles indicate 32 hits (cut off 3SD (standard deviation)). The numbers in color key indicate x times SD. ***D,*** Dendrogram of 32 hits. Circle size: normalized split-Rluc activity. Numbers in the parenthesis indicate false discovery rate (adjusted *p* values; see Experimental procedures).

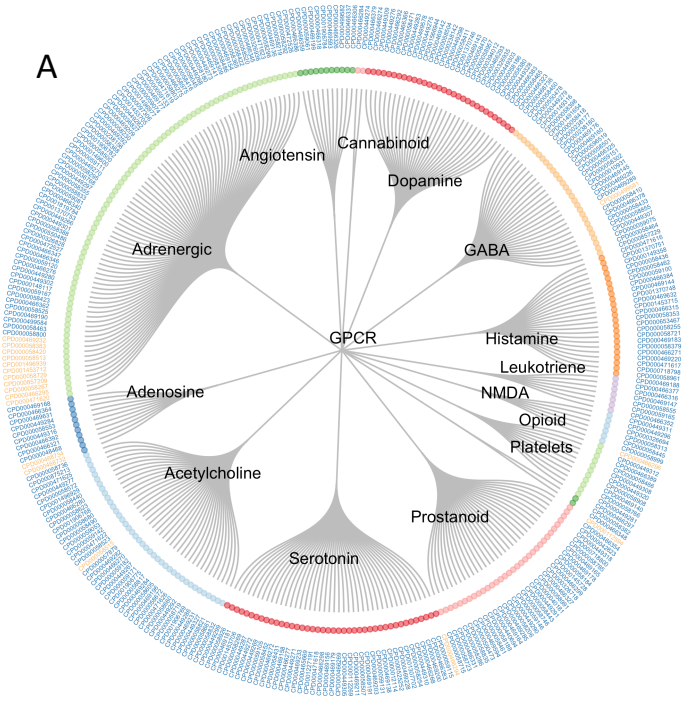

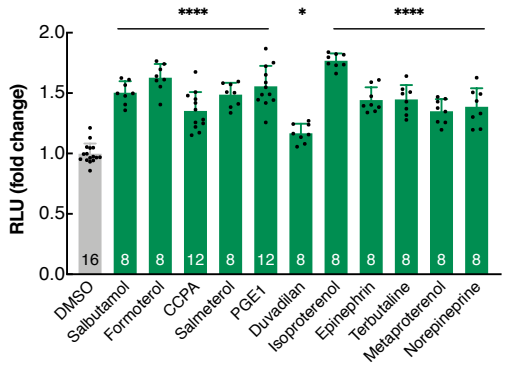

C

Structure_ID	Drug Name	Target GPCR	Receptor specificity
CPD000058267	Isoproterenol	AR	beta
CPD001453712	Metaproterenol	AR	beta
CPD000857209	Epinephrine	AR	alpha, beta
CPD001496939	Terbutaline	AR	beta-2
CPD000466295	Salmeterol	AR	beta-2
CPD000471620	Formoterol	AR	beta-2
CPD000058383	Norepinephrine	AR	alpha, beta
CPD000058513	Salbutamol	AR	beta-2
CPD000058729	Duvadilan	AR	beta
CPD000112594	Alprostadil (PGE1)	PGE2R	EP1, EP2
CPD000468732	CCPA	AdR	A1

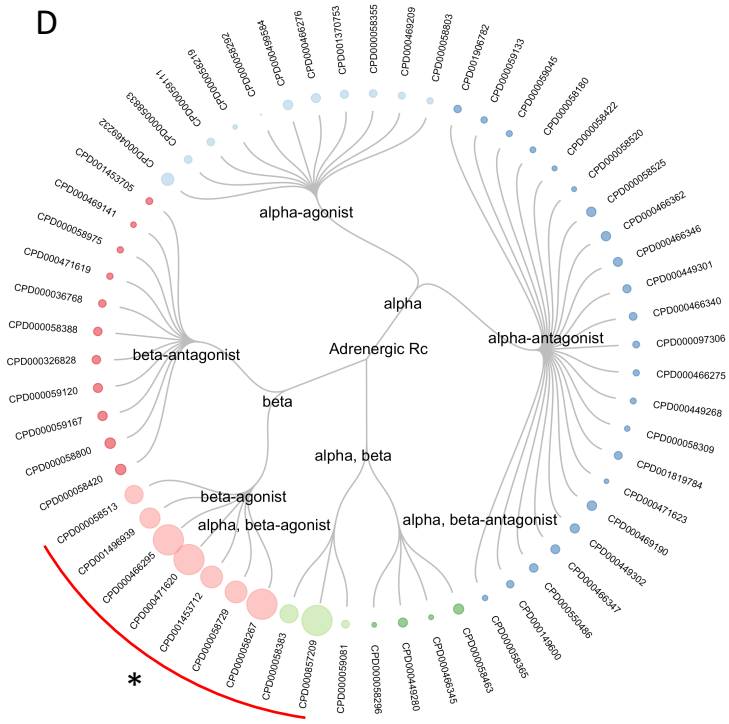

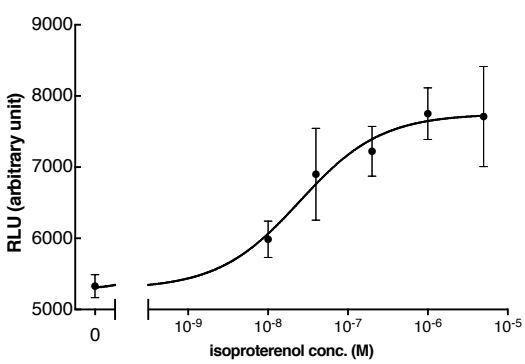

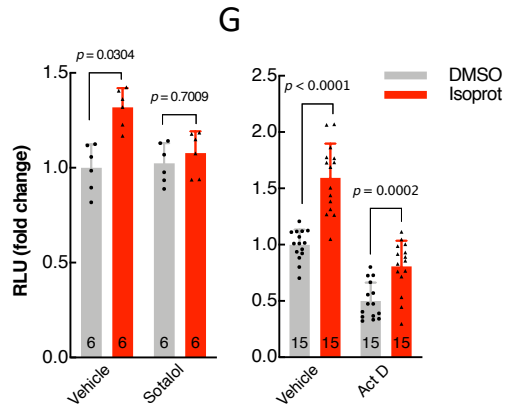

Figure 2. GPCR agonists increase reassembled split-Rluc activity in HEK293T cells. *A,* Circular dendrogram of all GPCR-associated drugs grouped into each pathway (Drug IDs orange color: 19 potential hits). ***B,*** Reassembled split-*Renilla* luciferase (split-Rluc) activities (RLU: relative light unit) of the DMSO and 11 confirmed hits (normalized to the mean of DMSO). Numbers at the bottom of each bar: sample numbers (*n*) from two independent experiments; 1-way ANOVA with Dunnett's multiple comparisons test; $^{*}p = 0.0137$; $^{****}p < 0.0001$). ***C,*** A list of 11 confirmed hits. AR: adrenergic receptor; AdR, adenosine receptor; CCPA, 2-chloro-N^{6}cyclopentyladenosine; PGE1, prostaglandin E1; PGE2R, PGE2 receptor. ***D,*** Circular dendrogram of all AR associated drugs. Circle size: normalized split-Rluc activity; circle color: target specificity; red curve with asterisk (*): 9 AR-associated hits. ***E,*** A concentration-responsive curve of isoproterenol effect on split-Rluc activity ($n = 16$ from two independent experiments; nonlinear regression (curve fit, sigmoidal function); Error bars: 95% CI. ***F-G,*** The effect of β-AR antagonist (sotalol, 250 μM) (F) and the transcription inhibitor actinomycin D (ActD, 0.8 μM) (G) on isoproterenol (isoprot)-induced split-Rluc activity. Numbers at the bottom of each bar: sample numbers (*n*) ; numbers at the top of each graph: *p* values (if ≤ 0.05, significant); 2-way ANOVA with Sidak's multiple comparisons test. All data: mean ± SD.

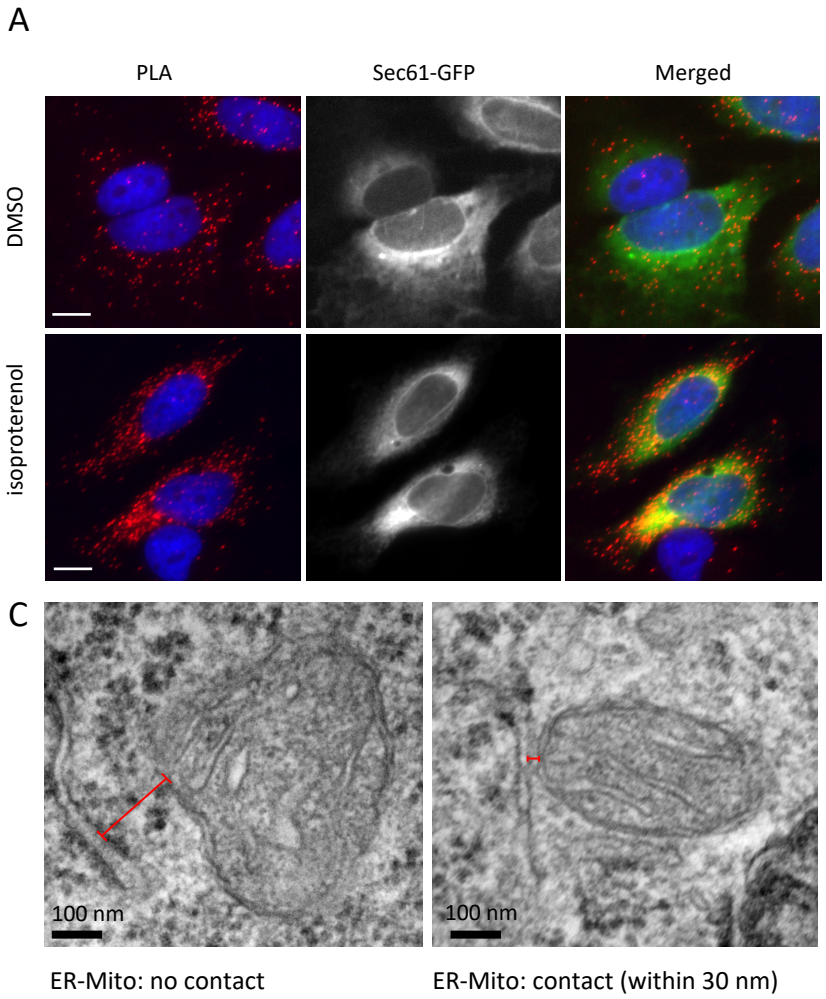

	No contact	Contact	Total
Control	268 (77.5%)	78 (22.5%)	346 (100%)
Isoprot	236 (58.3%)	169 (41.7%)	405 (100%)

Figure 3. GPCR agonists enhance physical contact between ER and mitochondria. ***A,*** Representative images of *in situ* proximity ligation assay (PLA) in HeLa cells treated with DMSO (top) or isoproterenol (1 μM) (bottom). PLA fluorescent signal (red) indicates a close apposition between ER and mitochondria. Sec61-GFP (green): to label ER; DAPI (blue): nucleus. Scale bars: 10 μm. ***B,*** Quantification of *in situ* PLA from HeLa cells treated with DMSO, isoproterenol (isoprot), CCPA, and PGE1 (1 μM each). Number of PLA puncta was counted in each cell and averaged across multiple cells (n = 81, 93 cells for DMSO, isoprot; n = 97, 96, 77 cells for DMSO, PGE1, CCPA; p values (if ≤ 0.05, significant) were determined by Mann-Whitney test (B-left); p values (if ≤ 0.05, significant) were determined by Kruskal-Wallis test with Dunn's multiple comparisons test (B-right). ***C,*** Representative transmission electron micrographs showing examples of mitochondrion that was counted as the one with no contact (left) or a close contact (right) with ER membrane in HEK293T cells. Red line depicts the distance measured between the outer mitochondrial membrane and ER membrane. Scale bars: 100 nm. ***D,*** Quantification of the percentage of ER-Mito contact in control vs isoproterenol (1 μM) treated cells (n = 339, 405 mitochondria for control, isoproterenol; Chi-square test; $p < 0.0001$). All data: mean ± SD.

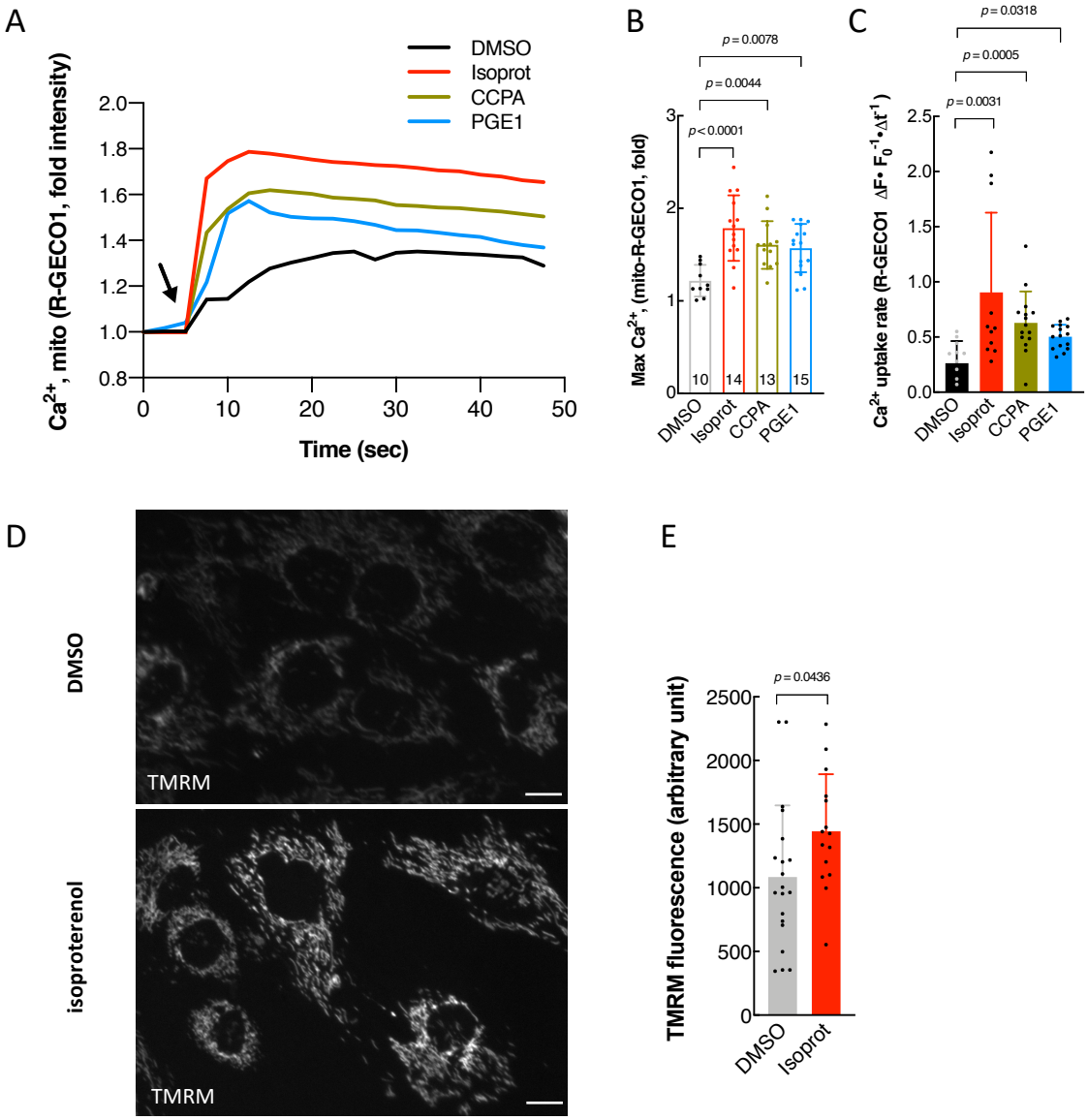

Figure 4. GPCR activation enhances mitochondrial Ca^{2+} uptake. ***A,*** Mitochondrial Ca^{2+} uptake in HeLa cells treated with DMSO, CCPA, isoproterenol (isoprot), or PGE1 (1 μM each), in response to ER Ca^{2+} release triggered by histamine (100 μM). Mito-R-GECO1 fluorescent intensity change ($\Delta F/F_0$) averaged across multiple cells is plotted for each drug (*n* = 10, 14, 13, and 15 cells for DMSO, isoprot, CCPA, and PGE1, from 3 experiments) every 2.5 sec (arrow indicates when histamine was added). ***B,*** Maximum peak mitochondrial Ca^{2+} uptake for each drug. Maximum mito-R-GECO1 fluorescent intensity change ($\Delta F/F_0$) averaged across multiple cells was normalized to that of DMSO and plotted as the fold change (from the same experiments in A). One-way ANOVA with Dunn's multiple comparisons test; *n* and *p* values: indicated in the graph). ***C,*** Mitochondrial Ca^{2+} uptake rate for each drug (from the same experiments in A; 7.5 to 12.5 sec). Kruskal-Wallis test with Dunn's multiple comparisons test; *n* (same as in B); *p* value of each drug (compared to DMSO): indicated in the graph; *p* value of each drug (compared to each other): *p* (isoprot vs. CCPA) = 0.3501, *p* (isoprot vs. PGE1) = 0.2023, *p* (CCPA vs. PGE1) = 0.9792. ***D,*** Representative images of TMRM (measuring mitochondrial membrane potential) fluorescent signal in HeLa cells treated with control or isoprot (1 μM). Scale bars: 10 μm. **E,** Quantification of TMRM fluorescence (*n* = 20, DMSO; *n* = 15, isoprot; unpaired two-tailed *t*-test with Welch's correction). All data: mean ± SD.

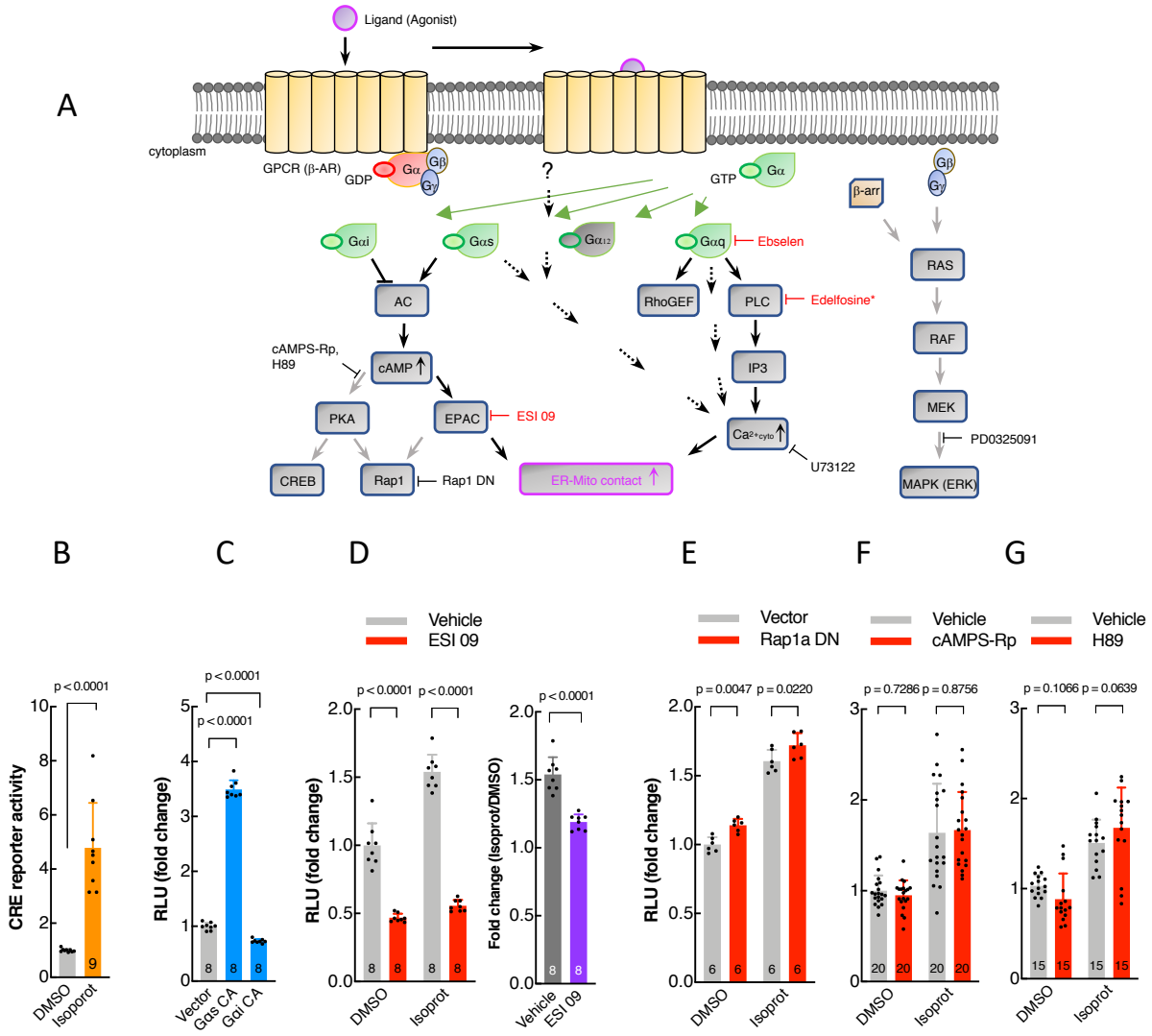

Figure 5. cAMP/EPAC pathway mediates agonist-induced β-AR signal for ER-Mito contacts. *A,* A schematic diagram of the GPCR pathway components (Note all the pathways are simplified). Downstream pathways involved (black) or not-involved (grey) in β-AR-mediated ER-Mito contact modulation are indicated with arrows (based on data in Fig. 5, 6); dotted arrows: uncertain pathways. Pathway Inhibitors are labeled with red (repressing) or black (not repressing) depending on their ability to repress isoproterenol-induced ER-Mito contacts. Asterisk (*): drug with an inhibitory trend (on isoproterenol-induced ER-Mito coupling) without reaching statistical significance. AC: adenylate cyclase; β-arr: β-arrestin; CREB: cAMP response element binding protein; EPAC: exchange protein directly activated by cAMP; G_α, G_β, and G_γ: α, β, and γ subunits of G-protein; PKA: protein kinase A; PLC: phospholipase C. ***B,*** cAMP response element (CRE) reporter gene assay in HEK293T cells treated with DMSO or isoproterenol (isoprot, 1 μM). Two-tailed unpaired *t*-test. ***C,*** Split-Rluc assay (RLU, relative light unit measuring luciferase activities; fold changes normalized to the mean of vector) in HEK293T cells transfected with vector (pCIG, expressing GFP), $G_{\alpha s}$ CA (constitutively active $G_{\alpha s}$ mutant), or $G_{\alpha i}$ CA (constitutively active $G_{\alpha i}$ mutant). One-way ANOVA with Dunnett's multiple comparisons test. ***D,*** (Left) Split-Rluc assay in H293T cells treated with vehicle vs ESI 09 (5 μM) in the presence of DMSO or isoproterenol (1 μM); 2-way ANOVA with Sidak's multiple comparisons test. (Right) Fold change of isoproterenol-induced luciferase activity (isoprot/DMSO) in the presence of vehicle vs. ESI 09 (using same data sets from the left graph); two-tailed unpaired *t*-test. ***E-G,*** Split-Rluc assay in HEK293T cells transfected with vector or Rap1a dominant negative (DN) construct (E), or treated with vehicle or PKA inhibitors (cAMPS-Rp, 10 μM; H89, 10 μM) (F, G), in the presence of DMSO or isoproterenol (1 μM); 2-way ANOVA with Sidak's multiple comparisons test. Numbers at the bottom of each bar: sample numbers (*n*); numbers at the top of each graph: *p* values (if ≤ 0.05, significant). All data: mean ± SD.

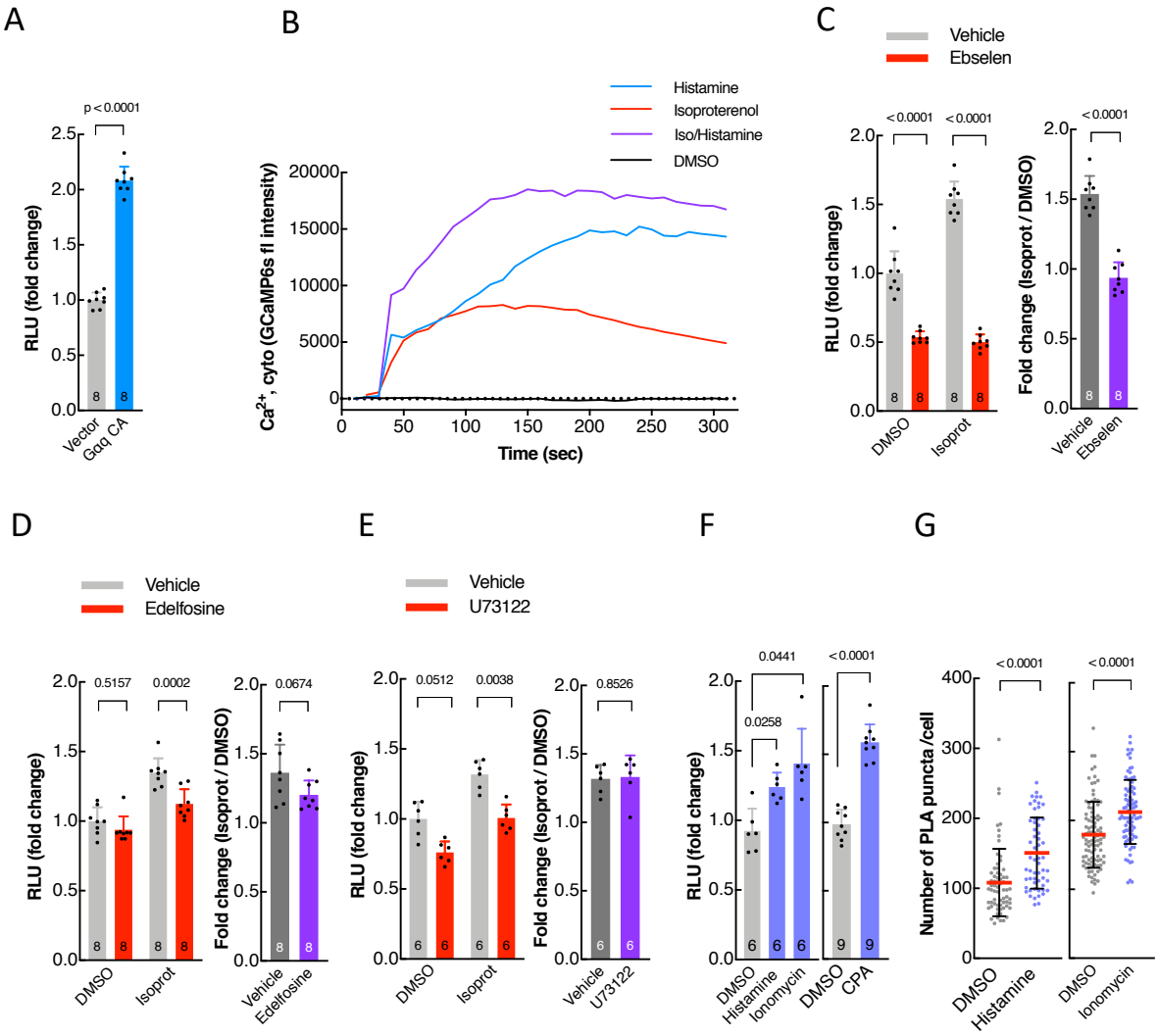

Figure 6. Elevated cytoplasmic Ca^{2+} enhances ER-Mito contact. *A,* Split-Rluc assay (fold change of the luciferase activity normalized to the mean of pCIG) in HEK293T cells transfected with the vector (pCIG), or Gαq CA (constitutively active Gαq); two-tailed unpaired *t*-test with Welch's correction. ***B,*** Cytoplasmic Ca^{2+} level measured by GCaMPs fluorescence intensity in HeLa cells treated with isoproterenol (1 μM), histamine (100 μM), or both, every 2.5 sec. Fluorescent intensity change ($\Delta F/F_0$) averaged across multiple cells is plotted for each treatment (n = 16). ***C-E,*** (Left): Split-Rluc assay in HEK293T cells treated with vehicle or indicated drugs (ebselen, 50 μM; edelfosine, 40 μM; or U73122, 5 μM), in the presence of DMSO or isoproterenol (1 μM). Fold change of the luciferase activity normalized to the mean of DMSO/Vehicle. 2-way ANOVA with Sidak's multiple comparisons test; (Right): Fold change of isoproterenol-induced luciferase activity (isoprot/DMSO) in the presence of vehicle vs. indicated drugs (using the same data sets from the left graphs in C-E); two-tailed unpaired *t*-test. F, Split-Rluc assay (fold change of the luciferase activity normalized to the mean of DMSO) in DMSO, histamine (100 μM), ionomycin (1 μM), or CPA (10 μM) treated HEK293T cells. 2-way ANOVA with Sidak's multiple comparisons test. ***F,*** Split-Rluc activities in DMSO, histamine (100 μM), ionomycin (1 μM), or CPA (10 μM) treated HEK293T cells (fold change normalized to the mean of DMSO). 1-way ANOVA with Dunn's multiple comparisons test (left); two-tailed paired *t*-test (right). ***G,*** Quantification of *in situ* PLA in HeLa cells (n = 66, 57, 97, 87 cells for DMSO, histamine, DMSO, ionomycin; Mann Whitney test). Numbers at the bottom of the bars: sample numbers (n); numbers at the top of the graphs: p values (if ≤ 0.05, significant). All data: mean ± SD.

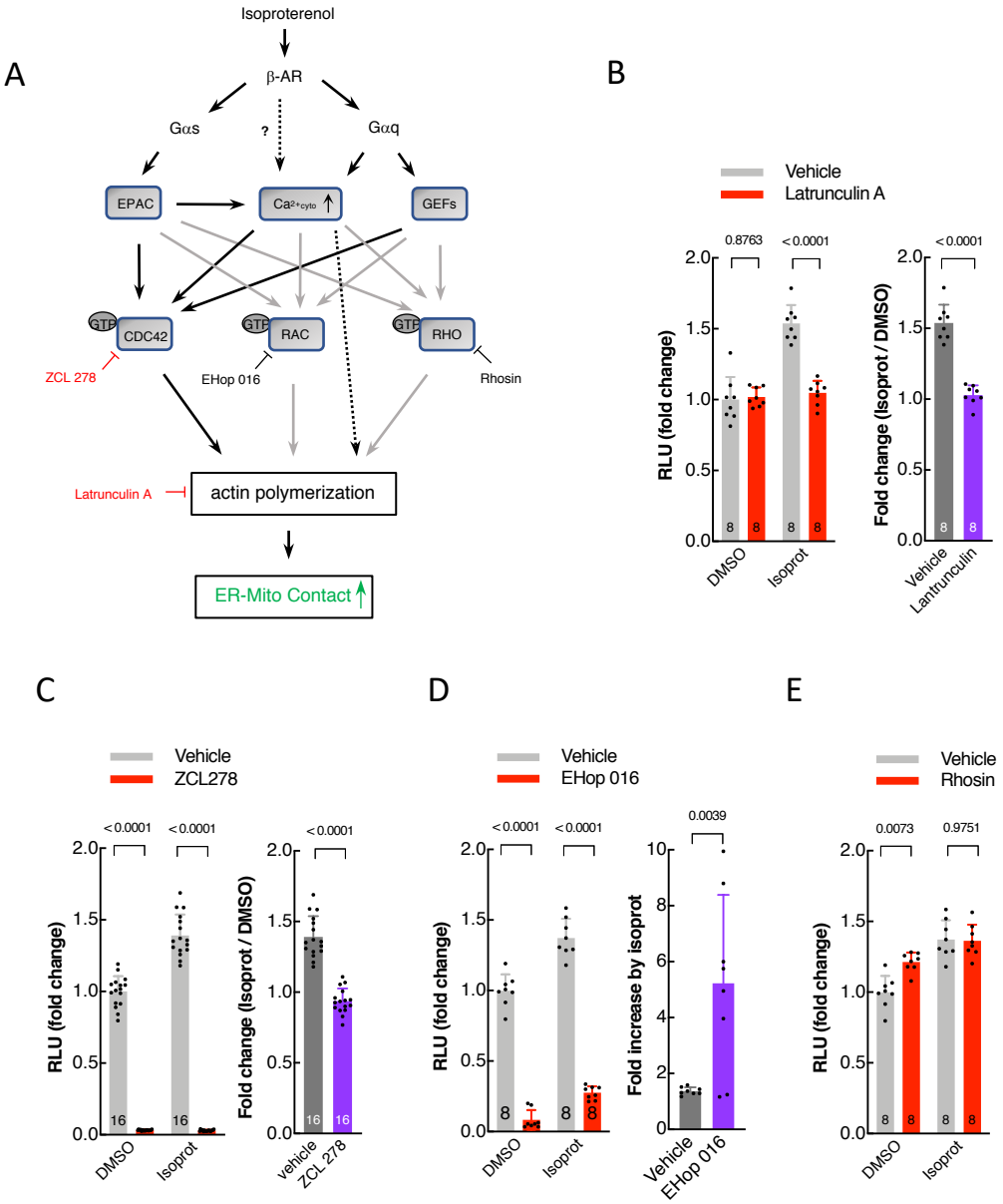

Figure 7. Actin polymerization is required for isoproterenol-mediated ER-Mito contact regulation. *A,* A schematic diagram (simplified) displaying the Rho GTPases and their upstream regulators potentially involved in actin polymerization required for isoproterenol-induced ER-Mito coupling. Pathways potentially involved (black) or not-involved (grey) in β-AR-mediated ER-Mito contact modulation are indicated with arrows (based on data in Fig. 5B-F and 6B-E); dotted arrows indicate unknown pathways. Drugs with red color indicate the ones blocked isoproterenol-induced split-Rluc activity, while black inhibitors did not. ***B-D,*** (Left): Split-Rluc assay in HEK293T cells treated with vehicle or indicated drugs (Latrunculin, 1 μM; ZCL 278, 25 μM; EHop 016, 12.5 μM) in the presence of DMSO or isoproterenol (1 μM). Fold changes: normalized to the mean of DMSO/vehicle. 2-way ANOVA with Sidak's multiple comparisons test. (Right): Fold change of isoproterenol-induced luciferase activity (isoprot/DMSO) in the presence of vehicle vs. indicated drugs (same data from the left graphs in B-D). Two-tailed unpaired *t*-test. ***E,*** Split-Rluc assay in HEK293T cells treated with vehicle or Rhosin (25 μM) in the presence of DMSO or isoproterenol (1 μM). Fold changes: normalized to the mean of DMSO/vehicle. 2-way ANOVA with Sidak's multiple comparisons test. Numbers at the bottom of the bars: sample numbers (*n*); numbers at the top of the graphs: *p* values (if ≤ 0.05, significant). All data: mean ± SD.

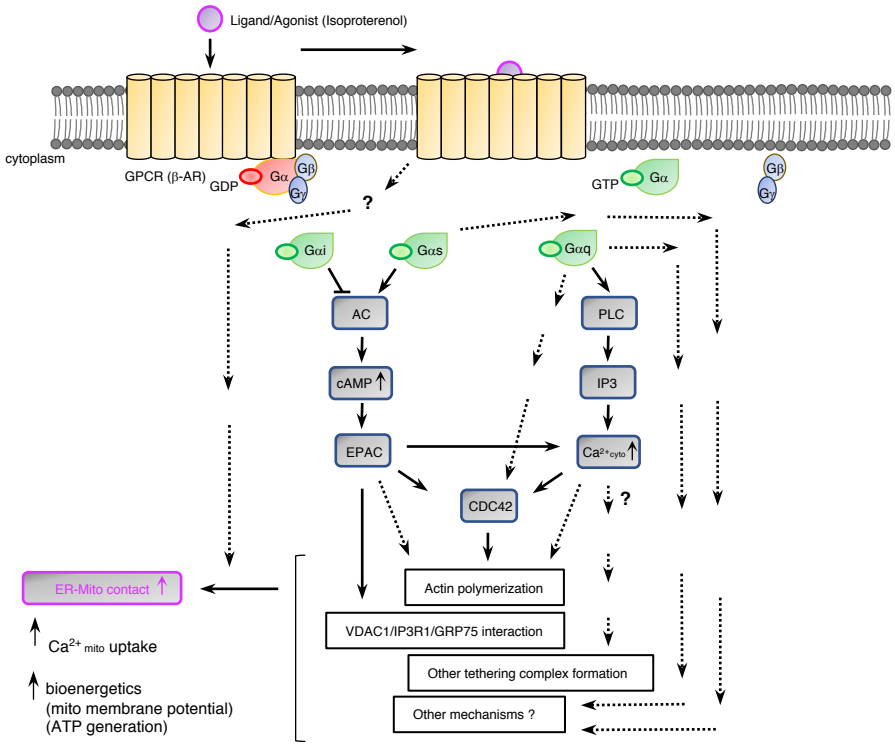

Figure 8. Proposed model for potential mechanisms of GPCR (β-AR) signaling in ER-Mito contact regulation. When isoproterenol stimulates β-AR, GTP-bound Gα dissociates from Gβ- and Gγ- subunits and activates downstream effectors, leading to increases in cAMP and cytosolic Ca^{2+}. We postulate that the increase in cAMP and subsequent activation of EPAC (a downstream effector of cAMP) facilitates ER-Mito interactions likely through 1) triggering actin polymerization mediated in our data by CDC42; and 2) inducing VDAC1/IP3R1/GRP75 interaction. Increased cytosolic Ca^{2+} can also increase ER-Mito interactions by influencing actin polymerization either through CDC 42 or unknown mechanism. It is also plausible that cAMP and Ca^{2+} might employ other mechanisms and that another pathway through β-AR might also participate in ER-Mito coupling (see dotted arrows).